Adiabatic temperature profile in the mantle, revised

Tomoo Katsura

Bayerisches Geoinstitut, University of Bayreuth, Universiaetsstrasse 30, 95447 Bayreuth, Germany.

Corresponding author: Tomoo Katsura (tomo.katsura@uni-bayreuth.de)

Key Points:

- The previous olivine-wadsleyite phase relations and P-V-T relations of mantle minerals are corrected using the pressure effect on EMF.
- Comparing the 410-km discontinuity depth with the olivine-wadsleyite phase relations suggests 1805(18) K at the discontinuity.
- The adiabatic temperatures are 1617(16) at 50-km depth and 2530(30) K at 2800-km depth.

Abstract

This study re-evaluates the adiabatic temperature profile of the Earth's mantle. The global average temperature at the 410-km discontinuity is estimated to be 1805(18) K by comparing the globally averaged depths of the 410-km discontinuity with the previously determined phase diagram of the olivine-wadsleyite transition in the system $(Mg,Fe)_2SiO_4$ at two temperatures. The temperature at the 410-km discontinuity is extrapolated to shallower and deeper regions using the adiabatic temperature gradient, which is estimated from the pressure-volume-temperature relations and heat capacities of the major mantle minerals, namely, olivine, wadselyite, ringwoodite, and bridgmanite. The experimental temperatures and pressures in the original studies used in these evaluations are re-calculated using the recently proposed pressure correction on EMF of the $W_{97}Re_3$-$W_{75}Re_{25}$ thermocouple. The uncertainties are evaluated by the Monte Carlo simulation. The temperatures on the adiabatic geotherm are found to be 1617(16), 1959(19), 1925(19), and 2530(30) K, respectively, at a 50-km depth, just above the 660-km discontinuity, just below the 660-km discontinuity, and a 2800-km depth. These temperatures are higher than those given by Katsura *et al.* (2010). The 50-km depth temperature is slightly higher but generally agrees to that estimated from the melting of depleted peridotite.

Plain Language Summary

This study estimates the temperature profile of the Earth's mantle by generally following the approach described in Katsura *et al.* (2010). The estimation consists of two steps. First, the temperature at the 410-km seismic discontinuity (D410), at which the seismic wave velocities abruptly increase almost everywhere in the mantle, is evaluated. The D410 is usually attributed to the olivine-wadsleyite transition in peridotite. Comparing the globally averaged D410 depth with the phase diagram of the olivine-wadsleyite transition yields the D410 temperature of 1805(18) K. Second, this temperature is extrapolated to shallower and deeper regions by assuming that the heat is mainly transferred by convection in the mantle. The temperature gradient in such cases is the product of the thermal expansion coefficient and the temperature divided by the density and the heat capacity. The thermal expansion coefficients of the major mantle mineral are obtained by recalculating our previous experimental data. We found that the temperatures at 50-km depth, the bottom of the mantle transition zone, the top of the lower mantle, and 2800-km depth are found 1617(16), 1959(19), 1925(19), and 2530(30) K, respectively. The 50-km depth temperature is slightly higher but generally agrees to that estimated from the melting of depleted peridotite.

1 Introduction

The temperature is one of the essential parameters for modeling the dynamics of the Earth's interior. Therefore, estimating the temperature distribution in the mantle is a vital task in solid geophysics. However, we cannot directly measure temperatures in the Earth's deep interior. We can only estimate the temperature distribution by combining various pieces of information obtained by indirect methods.

For this reason, Katsura *et al.* (2010) estimated the adiabatic temperature distribution in the mantle. They first estimated the temperature at the 410-km seismic discontinuity (D410) by comparing the global average depth of the D410 with the olivine-wadsleyite transition pressure as a function of temperature (Katsura *et al.*, 2004a). Then, they estimated the temperatures above and below the D410 using the formula of the adiabatic temperature gradient with depth as:

$$\left(\frac{dT}{dz}\right)_S = \frac{\alpha g T}{C_p} \quad (1)$$

where T is the temperature, z is the depth, α is the thermal expansivity of the constituent, g is the gravitational acceleration, and Cp is the isobaric heat capacity per weight of the constituent (Turcotte and Schubert, 2014). In their calculation, the mantle rocks were approximated by the Mg endmembers of olivine, wadsleyite, ringwoodite, and bridgmanite. The P-V-T relations of these minerals were determined using the multianvil in situ X-ray diffraction experiments by Katsura *et al.* (2004b; 2009a; 2009b; 2009c). The Cp for olivine, wadsleyite, and ringwoodite were taken from Saxena *et al.* (1993), and that for bridgmanite was calculated using the Debye model.

However, the adiabatic temperature profile by Katsura *et al.* (2010) has to be revised for the following reasons. First, the temperatures in Katsura *et al.* (2004a; 2004b; 2009a; 2009b; 2009c) were measured using $W_{97}Re_3$-$W_{75}Re_{25}$ thermocouples without any pressure correction. Nishihara *et al.* (2020) provided the pressure correction of the EMF-temperature relations of the $W_{97}Re_3$-$W_{75}Re_{25}$ thermocouple. Therefore, the experimental data in Katsura *et al.* (2004a; 2004b; 2009a; 2009b; 2009c) should be recalculated using Nishihara *et al.*'s (2020) correction. Second, Tange *et al.* (2012) obtained more reliable P-V-T data of $MgSiO_3$ bridgmanite than Katsura *et al.* (2009c). These data should be included in estimating the lower-mantle adiabatic profile. Third, the calculation program used in Katsura *et al.* (2010) was found to have errors leading to incorrect thermal expansivity evaluation, as shown later.

This paper presents a revised average adiabatic temperature profile in the mantle by integrating the above-mentioned new data and using a newly made calculation program.

2 Methods

The current study estimates an adiabatic temperature profile in the mantle by the procedure very similar to Katsura *et al.* (2010). Namely, it first estimates the temperature at D410, then estimates the temperature gradient, finally calculates the geotherm profile from the D410 temperature using the estimated temperature gradient. Details of the procedure are explained below.

2.1 Temperature at the 410-km discontinuity

The current study first considers the most probable global average of the D410 depth. Flanagan and Shearer (1998; 1999), Chambers *et al.* (2005), Houser *et al.* (2008; 2016) mapped the D410 depths globally and suggested the averaged depths of 418, 418, 409, 410, and 411 km, respectively. Although the older studies (Flanagan and Shearer, 1998; 1999) should have contained some uncertainties in absolute D410 depths due to the velocity structure variation of the crust, the recent two studies (Houser *et al.*, 2008; 2016) corrected them using the CRUST model (Mooney *et al.*, 1998). Therefore, the current study adopts the global average D410 depth of 410±1 km for the following calculation.

The current study employs the data given by Katsura *et al.* (2004a) for the phase relations of the olivine-wadsleyite transition in $(Mg,Fe)_2SiO_4$. They synthesized coexisting olivine and wadsleyite in a multi-anvil press with temperatures measured by $W_{97}Re_3$-$W_{75}Re_{25}$ thermocouples and pressures estimated from MgO volumes by *in situ* X-ray diffraction using the *P-V-T* relations of MgO suggested by Matsui *et al.* (2000). Then, Katsura *et al.* (2004a) measured the compositions of recovered olivine and wadsleyite grains using an electron probe microanalyzer (EPMA). In the current study, the temperatures in Katsura *et al.* (2004a) are corrected using Nishihara *et al.*'s (2020) pressure correction of the EMF-temperature relations. The pressures in Katsura *et al.* (2004a) are recalculated using these new temperatures and the two MgO equations of state (EOS) based on the 3rd-order Birch-Murnaghan EOS and Vinet EOS by Tange *et al.* (2009).

The recalculated olivine-wadsleyite phase-relation data are fitted to Strixrude's (1997) equations to express the binary loops at the above two temperatures. One essential parameter in his equations is the Fe-Mg partition coefficients between olivine and wadsleyite, $K_D^{\text{Mg-Fe}}$,

$$K_{\text{D}}^{\text{Mg-Fe}} = \frac{X_{\text{Fe}_2\text{SiO}_4}^{\text{Ol}} X_{\text{Mg}_2\text{SiO}_4}^{\text{Wd}}}{X_{\text{Fe}_2\text{SiO}_4}^{\text{Wd}} X_{\text{Mg}_2\text{SiO}_4}^{\text{Ol}}} \quad (2)$$

where X^j_i is the mole fraction of component *i* in phase *j*, and Π is the reduced pressure using the transition pressures of the endmembers of Mg_2SiO_4 and Fe_2SiO_4, $P\text{Mg}_2\text{SiO}_4$ and $P\text{Fe}_2\text{SiO}_4$, respectively as:

$$\Pi = \frac{P - P_{\text{Fe}_2\text{SiO}_4}}{P_{\text{Mg}_2\text{SiO}_4} - P_{\text{Fe}_2\text{SiO}_4}} \quad (3)$$

where *P* is the experimental pressure. The mole fraction of wadsleyite, f_{Wd}, is expressed as a function of Π with the parameter $K_D^{\text{Mg-Fe}}$ as:

$$f_{\text{wd}}(\Pi) = \frac{x_{\text{bulk}}\left(1 - K_{\text{D}}^{\text{Mg-Fe}}\right) - K_{\text{D}}^{\text{Mg-Fe}^{\Pi}} + K_{\text{D}}^{\text{Mg-Fe}}}{1 - K_{\text{D}}^{\text{Mg-Fe}^{1-\Pi}} - K_{\text{D}}^{\text{Mg-Fe}^{\Pi}} + K_{\text{D}}^{\text{Mg-Fe}}} \quad (4)$$

where xbulk is the bulk mole fraction of the Fe_2SiO_4 component. Fitting the experimental data to Eqs. (2) – (4) yields $K_D^{\text{Mg-Fe}}$, $P\text{Mg}_2\text{SiO}_4$ and $P\text{Fe}_2\text{SiO}_4$. Although Katsura *et al.* (2004a; 2010) assumed that the difference in the endmember transition pressures, $P\text{Mg}_2\text{SiO}_4$ - $P\text{Fe}_2\text{SiO}_4$, is independent of the temperature, this assumption is not adopted in the current study.

Similarly to Katsura *et al.* (2010), the current study assumes that the upper mantle is pyrolitic, namely, $X_{\text{Mg}} = 0.89$ (X_{Mg} = Mg/(Mg+Fe)) (Green and Falloon, 2009). Stixrude (1997) suggested that the D410 depth corresponds to the pressure where the olivine-to-wadsleyite ratio is 1:2, namely, $f_{\text{Wd}} = 2/3$. The current study follows this idea to obtain the olivine-wadsleyite transition pressure in the mantle peridotite ($P_{\text{Ol-Wd}}$) as a function of temperature. Comparing the pressure corresponding to the D410 depth with $P_{\text{Ol-Wd}}$ allows estimating the D410 temperature.

The uncertainties in the above estimations are evaluated using Monte Carlo simulation by producing 1000 replica sets of the phase relation data. This procedure produces the replica sets' data points, including pressure and compositions of olivine and wadsleyite, as:

$$x_i^j = x_i^0 + p \cdot \sigma_{x_i^0} \quad (5)$$

where x^j_i is the *i*-th data values in the *j*-th replica data set, x^0_i and σx^0_i are the average and standard deviation of the *i*-th datum in the original data set, and *p* is the normally distributed random number. Assuming the D410 depths of 409 and 411 km, the D410 temperatures are calculated for each replica set. The average and uncertainty of the D410 temperature are obtained from the mean value and standard deviation of the 1000 replica sets at the two D410 depths.

2.2 Evaluation of the parameters for the adiabatic temperature gradient

The adiabatic temperature gradient with pressure is given as:

$$\left(\frac{dT}{dP}\right)_S = \frac{\alpha T}{\rho_c C_P} \quad (6)$$

where ρ_c is the density of the constituent (Turcotte and Schubert, 2014). Therefore, evaluating the adiabatic temperature gradient requires the thermal expansivity, density, and isobaric heat capacity of the constituents as a function of pressure and temperature.

Following Katsura *et al.* (2010), the current study approximates the mantle constituents by the Mg-endmembers of olivine, wadsleyite, ringwoodite, and bridgmanite at depth ranges of 50-410, 410-520, 520-660, and 660-2800 km, respectively. Wolf *et al.* (2015) found that the adiabatic temperature gradients of $MgSiO_3$ and $(Mg_{0.83}Fe_{0.17})SiO_3$ bridgmanite are very similar, which supports the above approximation. On the other hand, although some studies suggested that the mantle transition zone contains weight percent levels of H_2O (Pearson *et al.*, 2014; Fei *et al.*, 2017), Houser (2016) predicted that the mantle transition zone is generally dry by combining the global analysis of long-period seismic data and the mineral physics data. Furthermore, the mantle transition zone is only 250-km thick and notably smaller than the whole mantle (2800 km thickness), and therefore, it should not change the temperature profile of the whole mantle significantly even if the transition zone were H_2O-rich.

The data sets for the density and thermal expansivity of olivine, wadsleyite, and ringwoodite are taken from Katsura *et al.* (2009a), Katsura *et al.* (2009b), and Katsura *et al.* (2004b), respectively. Those of bridgmanite are taken from Katsura *et al.* (2009c) and Tange *et al.* (2012). The temperatures of these data sets are recalculated using Nishihara *et al.*'s (2020) pressure correction on the thermocouple EMF. The pressures are then recalculated based on these new temperatures using the two MgO EOS's given by Tange *et al.* (2009).

The *P-V-T* data set of each mineral is fitted to the Mie-Grüneisen-Debye EOS (Jackson and Rigden, 1996) with the 3rd-order Birch-Murnaghan EOS (Katsura *et al.*, 2019). At the standard temperature of T_0 = 300 K, the 3rd-order Birch-Murnaghan EOS is expressed as:

$$P(V,T_0) = \frac{3}{2}K_{T_0}\left[\left(\frac{V_{P_0,T_0}}{V_{P,T_0}}\right)^{\frac{7}{3}} - \left(\frac{V_{P_0,T_0}}{V_{P,T_0}}\right)^{\frac{5}{3}}\right] \times \left\{1 - \frac{3}{4}\left(4 - K_{T_0}'\right)\left[\left(\frac{V_{P_0,T_0}}{V_{P,T_0}}\right)^{\frac{2}{3}} - 1\right]\right\} \qquad (7)$$

where $P(V, T_0)$ is the pressure at volume V and the standard temperature of T_0, K_{T0} is the isothermal bulk modulus at the temperature of T_0, K_{T0}' is its pressure derivative, and $V_{P0,T0}$ and $V_{P,T0}$ are the volume at the standard pressure of $P_0 = 0$ and at the pressure of P, respectively, under the temperature condition of T_0. The Mie-Grüneisen-Debye EOS is:

$$P(V,T) = P(V,T_0) + \frac{\gamma}{V}\left[E_{\mathrm{th}}(V_P,T) - E_{\mathrm{th}}(V_P,T_0)\right] \qquad (8)$$

where $P(V, T)$ is the pressure at the volume V and temperature T, γ is the Grüneisen parameter, and E_{th} is the thermal energy.

The volume dependence of the Grüneisen parameter is expressed using the constant q as:

$$\gamma = \gamma_0\left(\frac{V_{P,T}}{V_{P_0,T_0}}\right)^{q} \qquad (9)$$

where γ_0 is the Grüneisen parameter at the standard pressure P_0 and temperature T_0. The thermal energy, E_{th}, is given by:

$$E_{\mathrm{th}}(V,T) = \frac{9nRT}{(\theta/T)^3}\int_0^{\frac{\theta}{T}}\left(\frac{\xi^3}{e^{\xi}-1}\right)\mathrm{d}\xi \qquad (10)$$

where θ is the Debye temperature at the volume V, n is the number of atoms per formula unit, and R is the gas constant. The Debye temperature at the volume V is expressed as:

$$\theta = \theta_0 \exp\left[\frac{\gamma_0 - \gamma(V)}{q}\right] \quad (11)$$

where θ_0 is the Debye temperature at the standard volume V_0.

With the fixed values of K_{T0} and θ_0 given by literature (Isaak *et al.*, 1989; Mao *et al.*, 2008; Higo *et al.*, 2006; Tange *et al.*, 2012; Watanabe, 1982; Akaogi and Ito, 1993), the K_{T0}', γ_0, and q are fitted to minimize the sum of squared differences of the pressures based on each mineral's EOS, Pmineral, from those based on the MgO pressure marker using Tange *et al.*'s (2009) two EOS's, P_{MgO}. Namely, $\chi^2 = \Sigma(P_{mineral} - P_{MgO})^2$ is minimized.

The uncertainties of the fitting results of K_{T0}', γ_0, and q are evaluated using the Bootstrap method as follows. Firstly, 1000 bootstrap data sets are produced by randomly choosing data points from the original data set with allowing duplication. Then, uncertainties multiplied by the normally distributed random numbers are added to the individual data points using Eq. (5). The three parameters of K_{T0}', γ_0, and q are obtained by fitting the individual bootstrap data sets to the Eqs. (7) – (11). The averages and standard deviations of the three parameters are obtained from the mean values and standard deviations of the 1000 bootstrap data sets. Note that the Bootstrap method is not adopted in modeling the phase relations because the number of the data points for the phase relations is too small for the bootstrap method (3 pairs of olivine and wadsleyite compositions at each temperature).

The density at given pressure and temperature is evaluated from the ambient density divided by the relative volumes given by Eqs. (7) – (10). The thermal expansivity is obtained from the differentiation of the relative volumes with respect to the temperature.

It is assumed that the isochoric heat capacity, C_V, of olivine is independent of the pressure because of the high temperatures. Therefore, the isobaric heat capacity at high pressure, C_P, can be obtained using the isobaric heat capacity of olivine at ambient pressure, C_P^0 as:

$$C_P = (1 + \alpha\gamma T)C_V = (1 + \alpha\gamma T)\frac{C_P^0}{1+\alpha_0\gamma_0 T} = \frac{1+\alpha\gamma T}{1+\alpha_0\gamma_0 T}C_P^0 \quad (12)$$

where α and α_0 are the temperature-dependent thermal expansivities of olivine at high and ambient pressures, respectively. The isobaric heat capacity of olivine at ambient pressure is taken from Saxena *et al.* (1993), which was also adopted in Katsura *et al.* (2010).

The isobaric heat capacities of wadsleyite, ringwoodite and bridgmanite are obtained by multiplying the Debye heat capacity by $1 + \alpha\gamma T$.

2.3 Evaluation of adiabatic temperature profile in the Earth's mantle

The adiabatic temperature gradient to the depth (z) in the mantle is written as:

$$\left(\frac{dT}{dz}\right)_S = \rho_m g \left(\frac{dT}{dP}\right)_S \quad (13)$$

where ρ_m and g are the density and gravity acceleration at a certain depth of the Earth's mantle given by PREM (Dziewonski and Anderson, 1981). Note that the ρ_m in this equation is different from ρ_c in Eq. (6). The former is the density of the Earth's mantle, which consists of Fe-bearing peridotite. On the other hand, the latter is that of the Fe-free endmembers of the major mantle minerals. Katsura *et al.* (2010) did not consider this difference and simply obtained the adiabatic temperature gradient to the depth using Eq. (1), which is the major error source of Katsura *et al.* (2010).

Using Eq. (13), the temperatures at depths are obtained by 10-km increments and decrements from the D410 depth to deeper and shallower depths, respectively. It is well known that the latent heat associated with the phase transition of olivine to wadsleyite,

wadsleyite to ringwoodite, and ringwoodite to bridgmanite + ferropericlase abruptly changes the geotherm (Ito and Katsura, 1989, Katsura *et al.*, 2010). Following Katsura *et al.* (2010), the current study assumes the geotherm change of +60, +43, and -34 K by these transitions. Since the D410 is taken as the depth where the olivine and wadsleyite have a volume ratio of 1:2 (Stixrude, 1997), the temperature changes of +20 and -40 K are delivered above and below the D410, as Katsura *et al.* (2010) did. The wadsleyite to ringwoodite and ringwoodite to bridgmanite + ferropericlase transitions are assumed to occur at fixed depths of 520 and 660 km, respectively.

3 Results and discussion

3.1 Olivine-wadsleyite transition in $(Mg,Fe)_2SiO_4$

Table 1 presents the recalculated pressures and temperatures with the olivine and wadsleyite compositions from Katsura *et al.*'s (2004a) experiments. Figure 1 shows the recalculated phase relations of the olivine-wadsleyite transitions in $(Mg,Fe)_2SiO_4$. The Nishihara *et al.*'s (2020) pressure correction of thermocouple EMF has increased 1600 and 1900 K to 1644 and 1962 K, respectively. This correction has accordingly increased the pressures by 0.22 and 0.32 GPa at these temperatures, respectively. The fitting yields $K_D^{Mg\text{-}Fe}$ = 0.514±0.035, $P\mathrm{Mg_2SiO_4}$ = 14.12±0.13 GPa, and $P\mathrm{Fe_2SiO_4}$ = 3.6±1.0 GPa at 1962 K and $K_D^{Mg\text{-}Fe}$ = 0.598±0.036, $P\mathrm{Mg_2SiO_4}$ = 15.42±0.17 GPa, and $P\mathrm{Fe_2SiO_4}$ = 4.7±1.0 GPa at 1962 K. Consequently, the Clapeyron slopes of the Mg and Fe endmember transitions are 4.1±0.5 and 3.4±3.6 MPa/K, respectively. The uncertainties of $P\mathrm{Fe_2SiO_4}$ estimation (1.0 and 1.0 GPa) are 6~8 times larger than those of $P\mathrm{Mg_2SiO_4}$ (0.13 and 0.17 GPa). This is because Katsura *et al.* (2004a) conducted the experiments with the bulk compositions around X_{Mg} = 0.9. The estimated $P\mathrm{Mg_2SiO_4}$ and $P\mathrm{Fe_2SiO_4}$ are anticorrelated, as expected (Fig. S1).

Table 1. Temperature, Pressure, and Phase Compositions of Coexisting Olivine and Wadsleyite.

Run #	V/V_0^{MgO}	Temperature before Correction (K)	Pressure before Correction (GPa)	Temperature after Correction (K)	Pressure after Correction (GPa)	X_{Mg}^{Ol}	X_{Mg}^{Wd}
733	0.9738(6)	1900	14.24(16)	1964	14.64(16)	0.951(5)	0.923(1)
734	0.9763(3)	1900	13.78(11)	1962	14.18(11)	0.906(5)	0.852(7)
735	0.9788(3)	1900	13.33(10)	1961	13.71(10)	0.862(9)	0.792(3)
763	0.9741(5)	1600	12.29(13)	1643	12.56(13)	0.876(6)	0.782(6)
779	0.9785(5)	1600	13.33(14)	1645	13.62(14)	0.979(3)	0.947(6)
780	0.9725(6)	1600	12.58(15)	1643	12.86(15)	0.915(6)	0.840(4)

The initial data are from Katsura *et al.* (2004a).

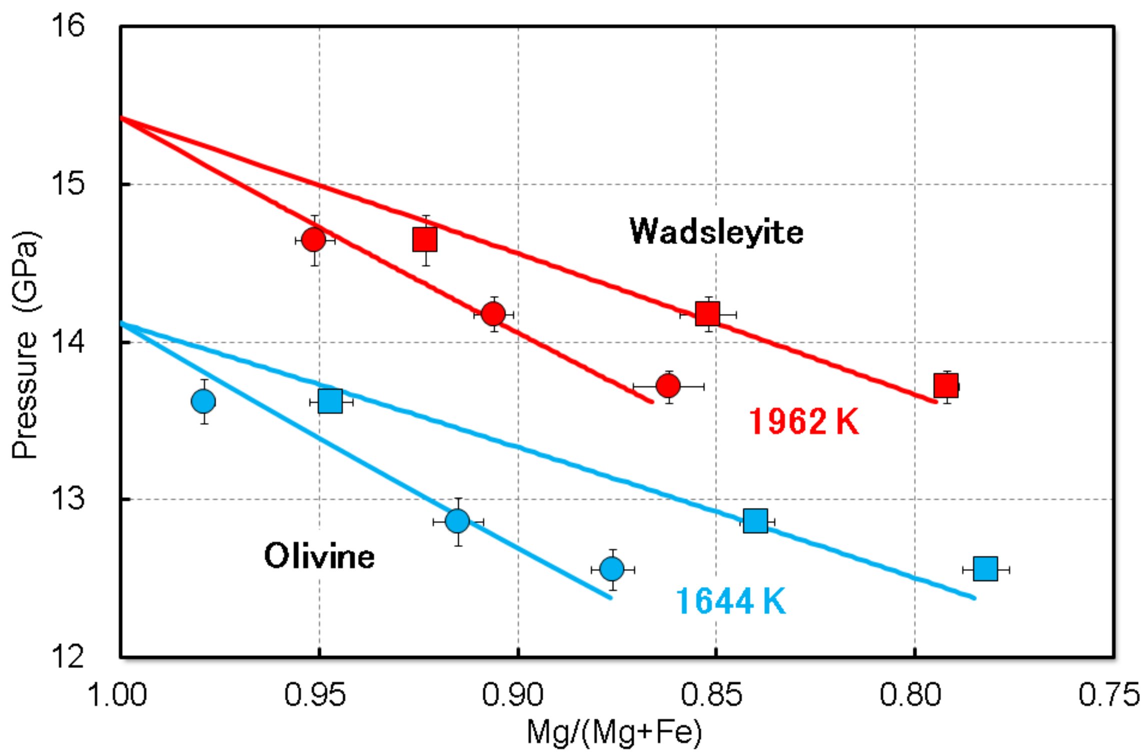

Figure 1. Binary phase relations of the olivine-wadsleyite transition in $(Mg,Fe)_2SiO_4$. The original data are from Katsura *et al.* (2004a). The temperatures were recalculated using Nishihara *et al.*'s (2020) pressure correction of the EMF-temperature relations of $W_{97}Re_3$-$We_{75}Re_{25}$ thermocouple. The temperatures of 1600 and 1900 K in Katsura *et al.* (2004a) became 1644 (blue) and 1962 (red) K. The circle and square symbols denote the compositions and pressures of coexisting olivine and wadsleyite, repectively.

Yagi *et al.* (1987) determined the fayalite-ahrensite transition in Fe_2SiO_4 using *in situ* X-ray diffraction with a multianvil press. Their data suggested $P_{Fe2SiO4}$'s of 7.0±0.1 and 6.2±0.1 GPa at 1644 and 1962 K, respectively, which are significantly higher than those estimated in the current study. Hence, the binary loop should have an old-crescent shape. However, these curvatures should be insignificant for the current study because the compositional range of Katsura *et al.* (2004a) already covers the mantle composition (X_{Mg} = 0.89 (Green and Falloon, 1998)) (Fig. 1).

3.2 Temperature at the 410-km discontinuity

The olivine-wadsleyite transition pressures in peridotite, $P_{Ol\text{-}Wd}$, are found to be 13.09±0.07 and 14.34±0.08 GPa at temperatures of 1644 and 1962 K, respectively. The smaller uncertainties in $P_{Ol\text{-}Wd}$ than $P_{Mg2SiO4}$ are because Katsura *et al.* (2004a) conducted the experiments with the bulk compositions around X_{Mg} = 0.9 and not at X_{Mg} = 1.0, or equivalently because the $P_{Mg2SiO4}$ and $P_{Fe2SiO4}$ are anticorrelated.

The temperature dependence of $P_{Ol\text{-}Wd}$, is $dP_{Ol\text{-}Wd}/dT$ = 3.9±0.3 MPa/K. This temperature dependence is significant because the temperature increase by 100 K causes the olivine-wadsleyite transition pressure to increase by 9.8±0.7 km. Comparing $P_{Ol\text{-}Wd}$ with the pressures of the D410 depths suggests the temperature at D410 to be 1805±18 K. That estimated by Katsura *et al.* (2010), 1830±48 K, was slightly higher than the present estimation. The reason for this difference is the thermocouple correction, which raises not only temperatures but also pressures of the experimental data points. The ratio of the pressure increase to the temperature increase is equal to the thermal pressure of MgO, which is 6.4 MPa/K at around 13 GPa and 1900~1600 K based on Tange *et al.* (2009). On the other hand, the temperature dependence of $P_{\text{Ol-Wd}}$ is smaller, *i.e.*, 3.9±0.3 MPa/K. As a result, the required temperature for the olivine-wadsleyite transition becomes lower by the thermocouple correction. Also, note that the uncertainty in the temperature estimation is smaller in the current study than in Katsura *et al.* (2010). This smaller uncertainty is because Katsura *et al.* (2010) did not consider the anticorrelation of P_{Mg2SiO4} and P_{Fe2SiO4}.

3.3 *P-V-T* relations of major mantle minerals

Tables S1-S4 show the recalculated *P-V-T* data of the four minerals. Table 2 presents the optimized values together with the assumed parameters. Figures S2-S5 show the comparisons of pressures obtained using the Tange *et al.*'s (2009) MgO EOSs and the EOS of each mineral in the current study.

The obtained *K*' of the four minerals are identical within the uncertainties (Table 2). A higher-pressure mineral has a larger γ_0. This is reasonable because, according to the definition, γ_0 is the rate of the pressure increase to the thermal energy increase at constant volume and ambient pressure. Since the thermal expansivity of minerals vastly increases with decreasing pressure below their stability fields, the pressure increase rate caused by the energy increase should be more significant at ambient pressure in higher-pressure minerals.

However, the relation between the stability field and *q* among different minerals is unclear due to the significant uncertainties. Although ringwoodite apparently has a larger *q* than wadsleyite (2.9±0.7 and 1.5±1.1), this difference is within the uncertainties. As expected, the γ_0 and *q* are strongly correlated, especially for wadsleyite and ringwoodite due to their narrow experimental pressure ranges. (Fig. S6). Consequently, the uncertainty in *q* has a relatively small effect on the estimations of density and thermal expansivity.

Table 2. Thermoelastic Parameters of the Major Mantle Minerals

Mineral	K_{T_0} (GPa)	K_{T_0}'	θ (K)	γ_0	q
Olivine	127.4[a]	4.2(4)	768[a]	1.00(2)	2.4(5)
Wadsleyite	169.2[b]	4.2(2)	814[c]	1.23(6)	1.5(11)
Ringwoodite	182.0[d]	4.8(4)	830[c]	1.34(6)	2.9(7)
Bridgmanite	256.7[e]	4.09(4)	1030[f]	1.53(3)	1.6(4)

a: Isaak *et al.* (1989); *b*: Mao *et al.* (2008); *c*: Watanabe *et al.* (1982); *d*: converted from K_S given by Higo *et al.* (2006) *e*: Tange *et al.* (2012); *f*: Akaogi and Ito (1993)

The obtained *K*' of the four minerals are identical within the uncertainties (Table 2). A higher-pressure mineral has a larger γ_0. This is reasonable because, according to the definition, γ_0 is the rate of the pressure increase to the thermal energy increase at constant volume and ambient pressure. Since the thermal expansivity of minerals vastly increases with decreasing pressure below their stability fields, the pressure increase rate caused by the energy increase should be more significant at ambient pressure in higher-pressure minerals.

However, the relation between the stability field and *q* among different minerals is unclear due to the significant uncertainties. Although ringwoodite apparently has a larger *q* than wadsleyite (2.9±0.7 and 1.5±1.1), this difference is within the uncertainties. As

expected, the γ_0 and q are strongly correlated, especially for wadsleyite and ringwoodite due to their narrow experimental pressure ranges. (Fig. S6). Consequently, the uncertainty in q has a relatively small effect on the estimations of density and thermal expansivity.

3.4 Adiabatic temperature profile in the Earth's mantle

Table 3 shows the adiabatic temperature profile in the mantle at depths from 50 to 2800 km obtained in the current study. Although the temperature profile in the real mantle should not be adiabatic in the lower-most region due to the thermal boundary layer, the present profile is constructed by ignoring the presence of the thermal boundary layer. Supplementary Table S5 shows various thermoelastic parameters at depths from 50 to 2800 km with a 10-km step. Among the shown parameters in Table S5, the density, gravitational acceleration, and pressure are taken from PREM (Dziewonski and Anderson, 1981). The other parameters are obtained through the procedure described above. The thermal expansivity, adiabatic temperature gradient, and adiabatic geotherm are plotted in Fig. 2, 3, and 4.

Table 3. Adiabatic Temperature Profile in the Earth's Mantle

Depth (km)	Pressure (GPa)	Temperature (K)	dT/dz (K/km)
50	1.5	1616(17)	0.54
70	2.1	1627(17)	0.52
90	2.8	1637(17)	0.50
100	3.1	1642(17)	0.50
120	3.8	1651(17)	0.48
140	4.4	1660(17)	0.46
160	5.1	1669(17)	0.45
180	5.8	1678(17)	0.44
200	6.4	1686(17)	0.43
220	7.1	1695(17)	0.42
240	7.8	1703(18)	0.41
260	8.5	1711(18)	0.40
280	9.2	1718(18)	0.39
300	9.9	1726(18)	0.38
320	10.6	1734(18)	0.38
340	11.2	1741(18)	0.37
360	11.9	1748(18)	0.36
380	12.6	1755(18)	0.35
400	13.4	1762(18)	0.34
410	13.7	1765(18)	0.34
410	13.7	1825(18)	0.35
420	14.1	1829(18)	0.36
440	14.9	1836(18)	0.35
460	15.6	1843(18)	0.35
480	16.4	1850(18)	0.35
500	17.1	1857(18)	0.34

520	17.9	1864(18)	0.34
520	17.9	1907(18)	0.34
540	18.7	1915(18)	0.39
560	19.5	1922(18)	0.38
580	20.3	1930(18)	0.38
600	21.0	1937(19)	0.37
620	21.8	1945(19)	0.37
640	22.6	1952(19)	0.36
660	23.4	1959(19)	0.35
660	23.4	1925(19)	0.35
700	25.2	1940(19)	0.39
800	29.6	1979(20)	0.38
1000	38.6	2051(21)	0.35
1200	47.8	2119(21)	0.33
1400	57.3	2182(22)	0.31
1600	66.9	2241(23)	0.29
1800	76.8	2296(24)	0.27
2000	86.9	2349(25)	0.26
2200	97.3	2399(26)	0.25
2400	108.0	2447(28)	0.24
2600	119.0	2494(30)	0.23
2800	130.4	2538(32)	0.22

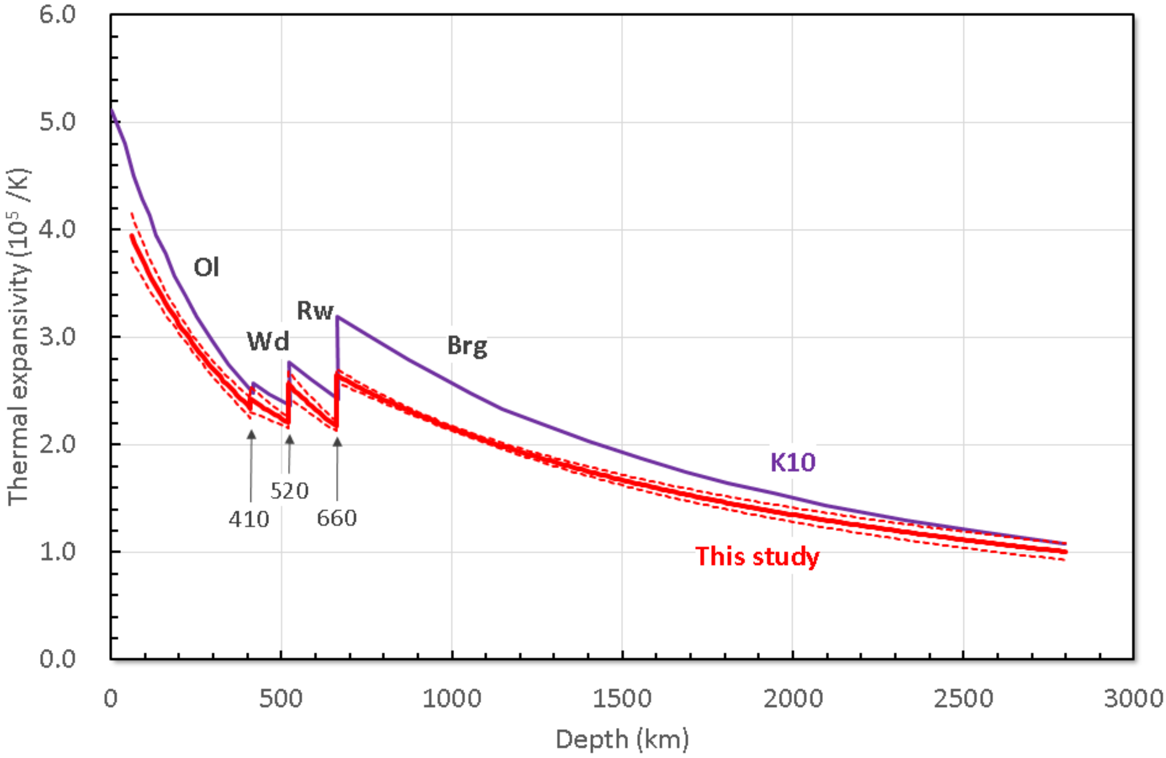

Figure 2. Thermal expansivity in the mantle. Red: the current study, violet: Katsura *et al.* (2010). The solid and dashed curves show the most probably and 68% confidence intervals, respectively.

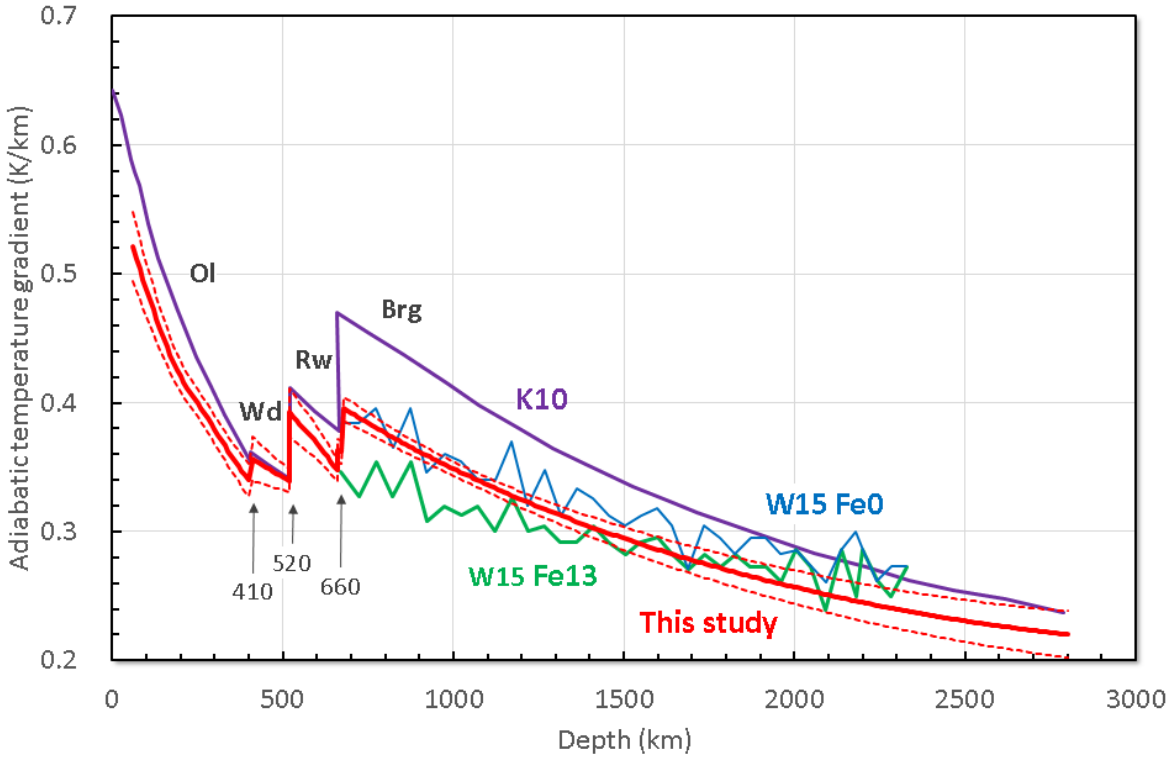

Figure 3. Adiabatic temperature gradients in the mantle. Red: the current study; violet: Katsura *et al.* (2010); blue: $MgSiO_3$ bridgmanite lower mantle by Wolf *et al.* (2015); green: $Mg_{0.87}Fe_{0.13}SiO_3$ bridgmanite lower mantle by Wolf *et al.* (2015). The solid and dashed curves show the most probably and 68% confidence intervals, respectively.

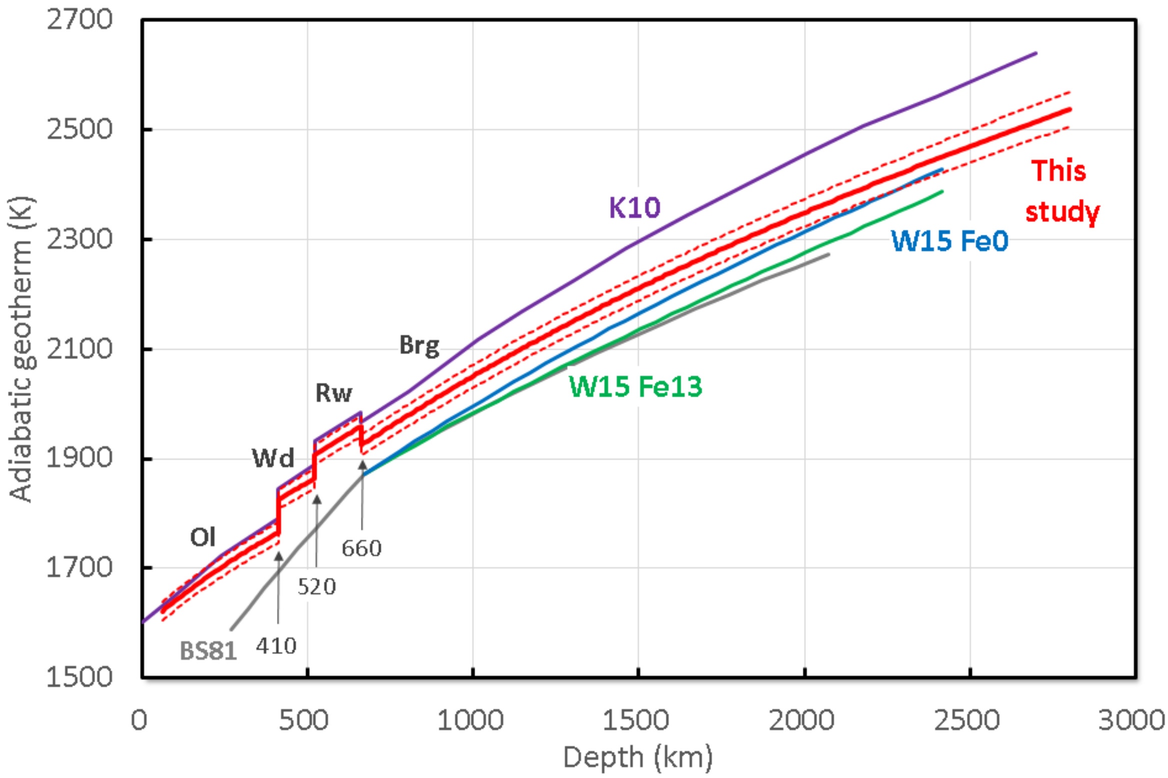

Figure 4. Adiabatic temperature profiles in the mantle. Red: the current study; violet: Katsura *et al.* (2010); blue: $MgSiO_3$ bridgmanite lower mantle by Wolf *et al.* (2015); green: $Mg_{0.87}Fe_{0.13}SiO_3$ bridgmanite lower mantle by Wolf *et al.* (2015); grey: Brown and Shankland (1981). The solid and dashed curves show the most probably and 68% confidence intervals, respectively.

As Katsura *et al.* (2010) argued, the thermal expansivity continuously decreases with increasing depth due to the negative temperature dependence when no phase transition occurs, whereas the phase transitions increase the thermal expansivity (Fig. 3). In the olivine stability field, the thermal expansivity decreases from $(4.0\pm0.2)\times10^{-5}$ to $(2.3\pm0.1)\times10^{-5}$ K^{-1} down to 410-km depth. In the wadsleyite and ringwoodite stability fields, it decreases from $(2.4\pm0.1)\times10^{-5}$ to $(2.2\pm0.5)\times10^{-5}$ and from $(2.6\pm0.1)\times10^{-5}$ to $(2.2\pm0.5)\times10^{-5}$ K^{-1}, respectively, at 410-520 and 520-660 km depths. In the bridgmanite stability field, it decreases from $(2.7\pm0.5)\times10^{-5}$ to $(1.0\pm0.1)\times10^{-5}$ K^{-1} to 2800-km depth. These values are about 10 % smaller than those of Katsura *et al.* (2010). Since the data sources are very similar between the current study and Katsura *et al.* (2010), Katsura *et al.* (2010) could have miscalculated the thermal expansivity.

Since the other parameters for the adiabatic temperature gradient given by Eq. (13) other than the thermal expansivity do not vary significantly, the adiabatic temperature gradient varies similarly to the thermal expansivity (Figs. 2 and 3). The adiabatic temperature gradient continuously decreases with depth without a phase transition, whereas it increases when a phase transition occurs. In the olivine stability field, the adiabatic gradient decreases from (0.53±0.03) to (0.35±0.01) K km^{-1} down to 410-km depth. In the wadsleyite and ringwoodite stability fields, it decreases from 0.36±0.02 to 0.34±0.01 and from 0.39±0.02 to 0.35±0.01 K km^{-1}, respectively, at 410-520 and 520-660 km depths. In the bridgmanite stability field, it decreases from 0.36±0.01 to 0.22±0.02 K km^{-1} to 2800-km depth. As expected, the current adiabatic gradient is smaller than Katsura *et al.* (2010), similarly to the thermal expansivity. On the other hand, the adiabatic gradient in the lower mantle from the current study agrees very well to those estimated by Wolf *et al.* (2015), which has gradients of 0.35-0.39 K/km at the top of the lower mantle and decrease to 0.25-0.27 K/km at 2300-km depth. Turcotte and Schubert (2014) suggested an adiabatic temperature gradient of 0.3 K km^{-1} in the mantle. This value may be a good approximation in the regions from the bottom of the upper mantle to the mid-mantle, but it may be underestimated for the uppermost mantle and overestimated for the deeper regions of the lower mantle.

According to the above argument, the temperatures are 1765±18 and 1825±18 K, respectively, just above and below the D410, 1864±18 and 1907±18 K, respectively, just above and below 520-km depth, and 1959±19 and 1925±19 K, respectively, just above and below 660-km depth (Table2, Fig. 4). The temperature at 50-km depth is 1616±17 K, whereas that at 2800-km depth is 2538±32 K. An extrapolation of the temperature at 50-km depth to the surface using the temperature gradient at 50-km depth (0.53 K km^{-1}) yields the mantle potential temperature of 1643 K (1370°C). These temperatures are lower than those of Katsura *et al.* (2010). One factor causing the lower temperature profile is that the temperature at D410 obtained in the current study is by 25 K lower than that of Katsura *et al.* (2010). More importantly, the temperature gradients of the current study are smaller than Katsura *et al.* (2010) (Fig. 3). As a result, the current study indicates *ca.* 120 K lower temperature at 2700 km depth than Katsura *et al.* (2010) (Fig. 4). Wolf *et al.* (2015) reported an adiabatic temperature profile in the lower mantle down to 2400-km depth. He suggested a temperature of 2390 K at 2400-km depth, which is 60 K lower than the current study (2450 K). This is because Wolf *et al.* (2015) arbitrarily assumed the temperature at 670-km depth of 1873 K, which is ca. 60 K higher than the present estimation (1929±29 K) (Fig. 4). Brown and Shankland (1981) estimated the adiabatic temperature profile and reported 90 K lower temperature at 2070 km depth (2359±26 K) than the current study (Fig. 5), which is also caused by the assumption of 1873 K at the top of the lower mantle in Brown and Shankland (1981).

Sarafian *et al.* (2017) determined the solidus temperature of mantle peridotite with 140 wt. ppm of H_2O at a pressure of 1.5 GPa, corresponding to 50 km depth. Their solidus temperature was 1590±10 K, which is slightly lower than that of the present profile, 1617±16 K. It is possible that the peridotite melting may start in the regions beneath mid-oceanic ridges slightly deeper than 50-km depth, and the melt finally separates from the source rocks at around 50 km depth.

Acknowledgments

The author thanks H. Fei, A. Chakraborti, F. Wang, L. Wang, and D. Bondar for reading and commenting on the manuscript. The current study is supported by the European Research Council (ERC) under Horizon 2020 research and innovation program (grant agreement No. 787527). There is no conflict of interest.

Open Research

The P-V-T data used in this study after the EMF correction using Nishihara et al. (2020) and the pressure calculation using Tange et al. (2009) are given at https://doi.org/10.5281/zenodo.5644426. The Matlab scripts to fit the P-V-T data to the equations of state, the temperature at the 410-km discontinuity, and calculate the adiabatic temperature profile are given at https://doi.org/10.5281/zenodo.5644430.

References

Akaogi, M., & Ito, E. (1993). Heat capacity of $MgSiO_3$ perovskite. *Geophysical Research Letters*, 20(2), 105–108. https://doi.org/10.1029/92GL02655

Brown, J.M., & Shankland, T.J. (1981). Thermodynamic parameters in the Earth as determined from seismic profiles. *Geophysical Journal of the Royal Astronomical Society*, 66(3), 579–596. https://doi.org/10.1111/j.1365-246X.1981.tb04891.x

Chambers, K., Woodhouse, J.H., & Deuss, A. (2005). Topography of the 410-km discontinuity from PP and SS precursors. *Earth and Planetary Science Letters* 235(3-4), 610–622. https://doi.org/10.1016/j.epsl.2005.05.014

Dziewonski, A.M., & Anderson, D.L. (1981). Preliminary reference earth model. *Physics of the Earth and Planetary Interiors*, 25(4), 297-356. https://doi.org/10.1016/0031-9201(81)90046-7

Fei, H., Yamazaki, D., Sakurai, M., Miyajima, N., Ohfuji, H., Katsura, T., Yamamoto, & T. (2017). A nearly water-saturated mantle transition zone inferred from mineral viscosity. *Science Advances*, 3(6), e1603024. https://doi.org/10.1126/sciadv.1603024

Flanagan, M.P., & Shearer, P.M. (1998). Global mapping of topography on transition zone velocity discontinuities by stacking SS precursors. *Journal of Geophysical Research: Solid Earth*, 103(B2), 2673–2692. https://doi.org/10.1029/97JB03212

Flanagan, M.P., & Shearer, P.M. (1999). A map of topography on the 410-km discontinuity from PP precursors. *Geophysical Research Letters* 26(5), 549–552. https://doi.org/10.1029/1999GL900036

Green, D.H., & Falloon, T.J. (1998). Pyrolite: A Ringwood Concept and Its Current Expression. In I. Jackson (Ed.), *The Earth's mantle* (pp.311-378). Cambridge University Press, Cambridge. https://doi.org/10.1017/CBO9780511573101.010

Higo, Y., Inoue, T., Li, B.S., Irifune, T., & Liebermann, R.C. (2006). The effect of iron on the elastic properties of ringwoodite at high pressure. *Physics of the Earth and Planetary Interiors,* 159(3-4), 276–285. https://doi.org/10.1016/j.pepi.2006.08.004

Houser, C., Masters, G., Flanagan, M., & Shearer, P. (2008). Determination and analysis of long-wavelength transition zone structure using SS precursors. *Geophysical Journal International* 174(1), 178–194. https://doi.org/10.1111/j.1365-246X.2008.03719.x

Houser, C. (2016). Global seismic data reveal little water in the mantle transition zone. *Earth Planetary Science Letters*, 448, 94-101. https://doi.org/10.1016/j.epsl.2016.04.018

Isaak, D.G., Anderson, O.L., Goto, T., & Suzuki, I. (1989). Elasticity of single-crystal forsterite measured to 1700 K. *Journal of Geophysical Research* 94, 5895–5906.

Ito, E., & Katsura, T. (1989). A temperature profile of the mantle transition zone. *Geophysical Research Letters* 16(5), 425-428. https://doi.org/10.1029/GL016i005p00425

Jackson, I., & Rigden, S.M. (1996). Analysis of P-V-T data: Constraints on the thermoelastic properties of high-pressure minerals. *Physics of the Earth and Planetary Interiors* 96(2-3), 85-112. https://doi.org/10.1016/0031-9201(96)03143-3

Katsura, T., Yamada, H., Kubo, A., Shinmei, T., Nishikawa, O., Yoshino, T., Aizawa, Y., Song, M.-s., Walter, M.J., Ito, E., & Funakoshi, K. (2004a). Olivine–wadsleyite transition in the system $(Mg,Fe)_2SiO_4$. Journal of Geophysical Research 109(2), B02209. https://doi.org/10.1029/2003JB002438

Katsura, T., Yokoshi, S., Song, M.-S., Kawabe, K., Tsujimura, T., Kubo, A., Ito, E., Tange, Y., Tomioka, N., Keiko, S., & Funakoshi, K. (2004b). Thermal expansion of Mg_2SiO_4 ringwoodite at high pressures. *Journal of Geophysical Research* 109(12), B12209. https://doi.org/10.1029/2004JB003094

Katsura, T., Shatskiy, A., Manthilake, M., Zhai, S.M., Fukui, H.,Yamazaki,D., Matsuzaki, T., Yoneda, A., Ito, E., Kuwata, A., Ueda, A., Nozawa, A., & Funakoshi, K. (2009a). Thermal expansion of forsterite at high pressures determined by in situ X-ray diffraction: the adiabatic geotherm in the upper mantle. *Physics of the Earth and Planetary Interiors*, 174(1-4), 86–92. https://doi.org/10.1016/j.pepi.2008.08.002

Katsura, T., Shatskiy, A., Manthilake, M., Zhai, S., Yamazaki, D., Matsuzaki, T., Yoshino, T., Yoneda, A., Ito, E., Sugita, M., Tomioka, N., Nozawa, A., & Funakoshi, K. (2009b). P-V-T relations of wadsleyite determined by in situ X-ray diffraction in a large-volume high-pressure apparatus. *Geophysical Research Letters* 36(11), L11307. https://doi.org/10.1029/2009GL038107

Katsura, T., Yokoshi, S., Kawabe, K., Shatskiy, A., Manthilake, M., Zhai, S.M., Fukui, H., Hegoda, H., Yoshino, T., Yamazaki, D., Matsuzaki, T., Yoneda, A., Ito, E., Sugita, M., Tomioka, N., Hagiya, K., Nozawa, A., & Funakoshi, K. (2009c). P-V-T relations of $MgSiO_3$ perovskite determined by in situ X-ray diffraction using a large-volume high-pressure apparatus. *Geophysical Research Letters* 36(1), L01305. https://doi.org/10.1029/2009GL039318

Katsura, T., Yoneda, A., Yamazaki, D., Yoshino, T., & Ito, E. (2010). Adiabatic temperature profile in the mantle. *Physics of the Earth and Planetary Interiors*, 183(1-2), 212-218. https://doi.org/10.1016/j.pepi.2010.07.001

Katsura, T., & Tange, Y. (2019). A Simple Derivation of the Birch-Murnaghan Equations of State (EOSs) and Comparison with EOSs Derived from Other Definitions of Finite Strain. *Minerals*, 9(12), 745. https://doi.org/10.3390/min9120745

Mao, Z., Jacobsen, S.D., Jiang, F., Smyth, J.R., Holl, C.M., Frost, D.J., & Duffy, T.S. (2008). Single-crystal elasticity of wadsleyites, β-Mg_2SiO_4, containing 0.37–1.66 wt.% H_2O. *Earth and Planetary Science Letters*, 266(1-2), 78–89. https://doi.org/10.1016/j.epsl.2007.10.045

Mooney, W.D., Laske, G., & Masters (1998). CRUST 5.1: A global crustal model at 5° × 5°. *Journal of Geophysical Research: Solid Earth* 103(1), 727–747. https://doi.org/10.1029/97JB02122

Matsui, M., Parker, S. C., & Leslie, M. (2000). The MD simulation of the equation of state of MgO: Application as a pressure calibration standard at high temperature and high pressure. *American Mineralogist* 85(2), 312-316. https://doi.org/10.2138/am-2000-2-308

Nishihara, Y., Doi, S., Kakizawa, S., Higo, Y., & Tange, Y. (2020). Effect of pressure on temperature measurements using WRe thermocouple and its geophysical impact. *Physics of the Earth and Planetary Interiors* 298, 106348. https://doi.org/10.1016/j.pepi.2019.106348

Pearson, D.G., Brenker, F.E., Nestola, F., McNeill, J., Nasdala, L., Hutchison, M.T., Matveev, S., Mather, K., Silversmit, G., Schmitz, S., Vekemans, B., & Vincze, L. (2014). Hydrous mantle transition zone indicated by ringwoodite included within diamond. *Nature* 507, 221-224. https://doi.org/10.1038/nature13080

Sarafian, E., Gaetani, G.A., Hauri, E.H., & Sarafian, A.R. (2017). Experimental constraints on the damp peridotite solidus and oceanic mantle potential temperature. *Science* 355(6328), 942-944. https://doi.org/10.1126/science.aaj2165

Saxena, S.K., Chtterjee, N., Fei, Y., & Shen, G. (1993). *Thermodynamic Data on Oxides and Silicates: An Assessed Data Set Based on Thermochemistry and High Pressure Phase Equilibrium* (pp. 428). Springer-Verlag, Berlin Heidelberg.

Stixrude, L. (1997). Structure and sharpness of phase transitions and mantle discontinuities. *Journal of Geophysical Research-Solid Earth* 102(7), 14835-14852. https://doi.org/10.1029/97JB00550

Tange, Y., Nishihara, Y. & Tsuchiya, T. (2009). Unified analyses for *P-V-T* equation of state of MgO: A solution for pressure-scale problems in high *P-T* experiments. *Journal of Geophysical Research-Solid Earth* 114(3), B03208. https://doi.org/10.1029/2008JB005813

Tange, Y., Kuwayama, Y., Irifune, T., Funakoshi, K., & Ohishi, Y. (2012). *P-V-T* equation of state of $MgSiO_3$ perovskite based on the MgO pressure scale: A comprehensive reference for mineralogy of the lower mantle. *Journal of Geophysical Research-Solid Earth* 117(6), B06201. https://doi.org/10.1029/2011JB008988

Turcotte, D. L., & Schubert, G. (2014), *Geodynamics*, 3rd edition, Cambridge University Press, Cambridge, pp. 1475.

Watanabe, H. (1982). Thermochemical Properties of Synthetic High-Pressure Compounds Relevant to the Earth's Mantle, in: A. S and M. MH (Eds.), *High-pressure Research in Geophysics*. Center for Academic Publications, Tokyo, pp. 441–464.

Wolf, A.S., Jackson, J.M., Dera, P., & Prakapenka, V.B. (2015). The thermal equation of state of (Mg, Fe)SiO_3 bridgmanite (perovskite) and implications for lower mantle structures. *Journal of Geophysical Research-Solid Earth*, 120(11), 7460-7489. https://doi.org/10.1002/2015JB012108

Yagi, T., Akaogi, M., Shimomura, O., Suzuki, T., & Akimoto, S.-I. (1987). In situ observation of the olivine-spinel phase transformation in Fe_2SiO_4 using synchrotron radiation. *Journal of Geophysical Research: Solid Earth*, 92(7), 6207-6213. https://doi.org/10.1029/JB092iB07p06207

Supplementary information

Table S1. *P-V-T* Data of Olivine

Table S2. *P-V-T* Data of Wadsleyite

Table S3. *P-V-T* Data of Ringwoodite

Table S4. *P-V-T* Data of Bridgmanite

Table S5. Thermoelastic Parameters Of The Adiabatic Mantle

Figure S1. Correlation of the Endmember Transition Pressures of the Olivine-Wadsleyite Transition.

Figure S2. Comparison of the Pressures using Tange *et al.*'s [2009] Mgo and the Current Study's Olivine EOS's.

Figure S3. Comparison of the Pressures using Tange *et al.*'s [2009] Mgo and the Current Study's Wadsleyite EOS's.

Figure S4. Comparison of the Pressures using Tange *et al.*'s [2009] Mgo and the Current Study's Ringwoodite EOS's.

Figure S5. Comparison of the Pressures using Tange *et al.*'s [2009] Mgo and the Current Study's Bridgmanite EOS's.

Figure S6. The Correlations of γ_0 and q.

Table S1. *P*-*V*-*T* data of olivine. The initial data is from Katsura et al. [2009a], and the pressure and tempeatures are recalcuted in this study.

Data #	T before correction (K)	V/V_0^{MgO}	P^{MgO} before correction (GPa)	T after correction (K)	V/V_0^{Ol}	P^{MgO} after correction (GPa)	P^{Ol} (GPa)	P^{MgO}-P^{Ol} (GPa)
M371008	1300	1.0371(2)	0.56(2)	1302	1.0300(3)	0.57(2)	0.37	-0.08
M371011	1100	1.0299(2)	0.27(3)	1101	1.0255(3)	0.27(3)	0.02	0.25
M371014	900	1.0227(1)	0.04(2)	900	1.0193(3)	0.04(2)	-0.10	0.14
M371017	700	1.0148(1)	-0.05(2)	700	1.0125(3)	-0.05(2)	-0.11	0.06
M371020	500	1.0069(1)	-0.02(2)	500	1.0051(3)	-0.02(2)	0.03	-0.05
M371023	304	0.9998(1)	0.06(2)	304	0.9996(3)	0.06(2)	0.07	-0.01
M371029	1300	1.0363(2)	0.66(3)	1303	1.0291(4)	0.67(3)	0.47	0.21
M371033	1300	1.0334(2)	1.05(3)	1304	1.0265(5)	1.07(3)	0.74	0.33
M371036	1500	1.0404(4)	1.39(6)	1507	1.0297(4)	1.43(6)	1.25	0.18
M371039	1700	1.0496(1)	1.49(2)	1709	1.0368(4)	1.54(2)	1.37	0.18
M375006	1300	1.0148(3)	3.66(6)	1312	0.9925(6)	3.74(6)	4.71	-0.97
M375009	1500	1.0250(2)	3.46(4)	1515	1.0047(4)	3.55(4)	4.01	-0.46
M375012	1300	1.0178(1)	3.23(3)	1311	1.0027(5)	3.30(3)	3.45	-0.15
M375015	1500	1.0236(2)	3.64(3)	1515	1.0061(5)	3.74(3)	3.85	-0.11
M375018	1300	1.0183(1)	3.15(3)	1311	1.0031(5)	3.22(3)	3.39	-0.18
M375021	1100	1.0134(1)	2.62(3)	1107	1.0013(4)	2.66(3)	2.81	-0.15
M375024	900	1.0090(1)	2.05(3)	904	0.9995(4)	2.07(3)	2.24	-0.17
M375027	700	1.0048(1)	1.47(2)	702	0.9985(4)	1.48(3)	1.60	-0.12
M375030	500	1.0011(1)	0.89(3)	501	0.9976(4)	0.90(3)	0.97	-0.07

M375033	305	0.9975(1)	0.42(2)	305	0.9967(4)	0.42(2)	0.43	-0.01
M375037	1500	1.0009(3)	7.06(7)	1526	0.9798(5)	7.22(7)	7.19	0.03
M375040	1700	1.0107(2)	6.80(4)	1731	0.9881(6)	6.99(4)	6.89	0.11
M375043	1500	1.0058(2)	6.28(4)	1524	0.9854(5)	6.42(4)	6.44	-0.01
M375046	1300	1.0008(2)	5.82(4)	1318	0.9825(5)	5.93(4)	6.02	-0.10
M375049	1100	0.9963(1)	5.30(3)	1112	0.9812(5)	5.37(3)	5.42	-0.05
M375052	900	0.9923(1)	4.71(3)	908	0.9798(5)	4.76(3)	4.84	-0.08
M375055	700	0.9883(1)	4.17(3)	705	0.9787(5)	4.20(3)	4.25	-0.05
M375058	500	0.9848(1)	3.59(2)	503	0.9777(5)	3.61(2)	3.66	-0.05
M375061	308	0.9815(1)	3.15(3)	309	0.9771(5)	3.16(3)	3.12	0.03
M375067	1700	0.9838(2)	11.18(7)	1745	0.9570(5)	11.46(7)	11.27	0.19
M375070	1900	0.9923(2)	10.99(7)	1954	0.9636(6)	11.33(7)	11.07	0.26
M375073	1700	0.9867(3)	10.66(8)	1743	0.9596(5)	10.93(8)	10.87	0.07
M375076	1500	0.9830(2)	10.05(7)	1533	0.9578(5)	10.26(7)	10.35	-0.10
M375079	1300	0.9786(2)	9.57(6)	1325	0.9554(5)	9.73(6)	9.96	-0.23
M375082	1100	0.9747(2)	9.04(6)	1119	0.9541(5)	9.15(6)	9.40	-0.25
M375085	900	0.9699(2)	8.68(5)	913	0.9528(5)	8.76(5)	8.88	-0.12
M375088	700	0.9663(2)	8.14(5)	709	0.9519(5)	8.19(5)	8.30	-0.10
M375091	500	0.9628(2)	7.65(4)	505	0.9508(4)	7.68(4)	7.77	-0.09
M375094	309	0.9598(2)	7.23(4)	312	0.9502(4)	7.24(4)	7.27	-0.03
M375100	1500	0.9679(3)	12.81(10)	1539	0.9417(5)	13.06(10)	12.94	0.11
M375103	1700	0.9729(3)	13.15(11)	1750	0.9448(6)	13.47(11)	13.19	0.28
M375106	1900	0.9840(2)	12.40(8)	1958	0.9534(6)	12.77(8)	12.60	0.16
M375109	1700	0.9801(2)	11.83(8)	1746	0.9514(5)	12.12(8)	12.14	-0.01

M375112	1500	0.9756(2)	11.38(7)	1536	0.9491(5)	11.61(8)	11.73	-0.12
M375115	1300	0.9710(2)	10.98(7)	1328	0.9476(5)	11.16(7)	11.20	-0.04
M375118	1100	0.9668(2)	10.51(6)	1121	0.9457(5)	10.64(7)	10.76	-0.12
M375121	900	0.9627(2)	10.07(6)	915	0.9443(5)	10.16(6)	10.27	-0.11
M375124	700	0.9590(2)	9.58(5)	710	0.9433(5)	9.63(5)	9.71	-0.07
M375127	500	0.9553(1)	9.15(4)	506	0.9422(4)	9.18(4)	9.22	-0.03
M375130	309	0.9520(1)	8.81(3)	312	0.9402(4)	8.83(3)	8.97	-0.14
M375135	1700	0.9716(4)	13.37(12)	1750	0.9444(5)	13.69(13)	13.26	0.43

The original data are from Katsura *et al.* [2009a].

Table S2. *P-V-T* data of wadsleyite. . The initial data is from Katsura et al. [2009b], and the pressure and tempeatures are recalcuted in this study.

Data #	T before correction (K)	V/V_0^{MgO}	P^{MgO} before correction (GPa)	T after correction (K)	V/V_0^{Wd}	P^{MgO} after correction (GPa)	P^{Wd} (GPa)	P^{MgO}-P^{Wd}(GPa)
M306028	1500	0.9650(1)	13.38(8)	1540	0.9566(2)	13.64(9)	13.72	-0.08
M306030	1500	0.9661(1)	13.17(8)	1540	0.9572(1)	13.42(9)	13.58	-0.16
M306033	1600	0.9697(1)	13.08(8)	1645	0.9602(2)	13.37(8)	13.46	-0.09
M306041	1700	0.9681(1)	14.05(9)	1752	0.9578(1)	14.38(9)	14.46	-0.08
M306044	1600	0.9649(1)	14.03(9)	1647	0.9556(1)	14.32(9)	14.41	-0.09
M306047	1500	0.9623(1)	13.90(9)	1541	0.9539(1)	14.17(9)	14.30	-0.13
M306050	1400	0.9599(1)	13.75(9)	1437	0.9523(1)	13.98(9)	14.15	-0.17
M306053	1300	0.9577(1)	13.56(8)	1332	0.9509(1)	13.76(9)	13.97	-0.21
M306056	1100	0.9531(1)	13.23(8)	1124	0.9483(1)	13.38(8)	13.57	-0.19
M306059	900	0.9486(1)	12.92(7)	917	0.9459(1)	13.03(7)	13.17	-0.14
M306062	700	0.9445(1)	12.57(5)	712	0.9437(1)	12.64(6)	12.75	-0.11
M306065	500	0.9407(1)	12.23(4)	507	0.9419(1)	12.27(4)	12.29	-0.02
M306068	309	0.9376(1)	11.92(4)	313	0.9405(1)	11.94(4)	11.87	0.07
M306071	308	0.9349(10)	12.53(26)	312	0.9383(1)	12.54(26)	12.38	0.17
M306073	1700	0.9622(1)	15.19(10)	1754	0.9524(2)	15.54(11)	15.61	-0.07
M306078	316	0.9313(1)	13.38(4)	320	0.9336(1)	13.40(4)	13.53	-0.13
M307010	1500	0.9493(0)	16.55(11)	1546	0.9476(1)	16.84(11)	16.66	0.03
M307013	1700	0.9565(1)	16.33(11)	1757	0.9441(1)	16.69(12)	16.45	-0.20
M307016	1500	0.9521(1)	15.96(11)	1545	0.9418(1)	16.24(11)	15.99	-0.17

M307019	1300	0.9478(1)	15.60(10)	1335	0.9395(1)	15.82(10)	15.57	-0.16
M307022	1100	0.9436(1)	15.25(9)	1126	0.9374(1)	15.41(9)	15.11	-0.12
M307025	900	0.9396(1)	14.87(7)	919	0.9353(1)	14.99(8)	14.70	-0.11
M307028	700	0.9358(1)	14.51(6)	713	0.9336(1)	14.58(6)	14.23	-0.05
M307031	500	0.9323(1)	14.13(5)	508	0.9324(1)	14.17(5)	13.77	0.08
M307034	306	0.9292(1)	13.83(3)	310	0.9524(1)	13.85(3)	14.61	-0.16
M307039	1500	0.9609(0)	14.19(9)	1542	0.9566(1)	14.45(9)	14.22	-0.02
M307042	1600	0.9656(1)	13.90(9)	1646	0.9556(1)	14.19(9)	13.92	-0.08
M307045	1500	0.9639(1)	13.58(9)	1541	0.9530(1)	13.84(9)	13.50	-0.15
M307048	1300	0.9597(1)	13.16(8)	1331	0.9506(1)	13.36(8)	13.06	-0.16
M307051	1100	0.9555(1)	12.75(7)	1123	0.9486(1)	12.90(7)	12.57	-0.17
M307054	900	0.9516(1)	12.30(6)	917	0.9467(1)	12.40(6)	12.06	-0.03
M307057	700	0.9474(1)	11.96(5)	711	0.9451(1)	12.03(5)	11.54	0.00
M307060	500	0.9440(1)	11.50(4)	507	0.9439(1)	11.54(4)	11.08	0.08
M307063	305	0.9411(1)	11.14(3)	309	0.9388(1)	11.16(3)	17.67	-0.13
M308012	1500	0.9461(1)	17.24(12)	1547	0.9328(1)	17.54(12)	14.42	-0.10
M308014	1500	0.9468(1)	17.08(12)	1547	0.9322(1)	17.38(12)	13.84	0.06
M308017	1600	0.9500(1)	17.04(12)	1653	0.9408(1)	17.38(12)	18.19	-0.04
M308020	1700	0.9533(1)	16.98(12)	1758	0.9388(2)	17.35(12)	17.66	0.07
M308025	1700	0.9543(1)	16.78(12)	1758	0.9363(1)	17.14(12)	17.27	-0.07
M308028	1500	0.9499(1)	16.42(11)	1546	0.9341(1)	16.71(11)	16.83	-0.10
M308031	1300	0.9458(1)	16.04(10)	1336	0.9322(1)	16.26(10)	16.34	-0.20
M308034	1100	0.9419(1)	15.62(9)	1127	0.9304(1)	15.78(9)	15.86	-0.21
M308037	900	0.9385(0)	15.11(7)	919	0.9293(1)	15.23(8)	15.28	-0.06

M308040	700	0.9351(0)	14.66(6)	713	0.9278(1)	14.73(6)	14.91	-0.09
M308043	500	0.9316(1)	14.28(5)	508	0.9382(1)	14.33(5)	18.80	0.25
M308046	307	0.9290(1)	13.88(4)	311	0.9360(2)	13.90(4)	18.32	0.13
M308050	1700	0.9495(1)	17.77(13)	1760	0.9334(1)	18.15(13)	17.96	-0.03
M308054	1500	0.9451(1)	17.43(12)	1548	0.9315(1)	17.74(12)	17.46	-0.10
M308057	1300	0.9415(1)	16.97(11)	1337	0.9296(1)	17.20(11)	16.97	-0.11

The original data are from Katsura *et al.* [2009b].

Table S3. *P*-*V*-*T* data of ringwoodite. . The initial data is from Katsura et al. [2004b], and the pressure and tempeatures are recalcuted in this study.

Data #	T before correction (K)	V/V_0^{MgO}	P^{MgO} before correction (GPa)	T after correction (K)	V/V_0^{Rw}	P^{MgO} after correction (GPa)	P^{Rw} (GPa)	P^{MgO}-P^{Rw} (GPa)
M038090	1500	0.9263(4)	21.71(18)	1554	0.9300(3)	22.05(19)	21.69	0.37
M038092	1550	0.9278(3)	21.67(18)	1607	0.9311(3)	22.03(19)	21.68	0.35
M038094	1600	0.9291(3)	21.69(18)	1661	0.9316(3)	22.08(19)	21.83	0.25
M038096	1650	0.9306(2)	21.66(17)	1714	0.9321(2)	22.06(18)	21.96	0.10
M038098	1700	0.9317(3)	21.71(18)	1767	0.9328(3)	22.14(19)	22.06	0.07
M038100	1600	0.9301(3)	21.46(18)	1660	0.9318(2)	21.84(18)	21.75	0.09
M038102	1500	0.9283(3)	21.24(17)	1554	0.9306(2)	21.58(17)	21.53	0.05
M038104	1400	0.9265(3)	21.03(16)	1447	0.9296(2)	21.33(17)	21.24	0.10
M038106	1300	0.9247(3)	20.83(16)	1342	0.9282(3)	21.10(16)	21.08	0.02
M038108	1200	0.9227(2)	20.66(14)	1236	0.9271(2)	20.89(15)	20.85	0.04
M038111	1100	0.9211(2)	20.43(13)	1131	0.9256(3)	20.63(13)	20.74	-0.11
M038113	1000	0.9191(2)	20.29(13)	1027	0.9243(3)	20.46(13)	20.55	-0.09
M038115	900	0.9171(2)	20.16(12)	923	0.9236(2)	20.30(12)	20.24	0.05
M038117	800	0.9156(3)	19.93(12)	819	0.9223(2)	20.04(13)	20.11	-0.07
M038119	700	0.9138(3)	19.76(11)	715	0.9212(1)	19.86(11)	19.94	-0.08
M038121	600	0.9120(3)	19.62(11)	612	0.9202(2)	19.70(11)	19.74	-0.05
M038123	500	0.9104(3)	19.45(10)	510	0.9190(1)	19.51(11)	19.62	-0.11
M038125	400	0.9091(4)	19.25(12)	407	0.9181(2)	19.29(12)	19.46	-0.17
M038127	300	0.9084(4)	18.96(11)	305	0.9180(2)	18.98(11)	19.12	-0.14

M038129	1700	0.9322(3)	21.59(19)	1767	0.9331(2)	22.02(19)	21.97	0.05
M038130	1750	0.9325(3)	21.85(18)	1821	0.9337(2)	22.31(19)	22.10	0.21
M038132	1800	0.9348(4)	21.65(19)	1874	0.9348(2)	22.13(20)	22.11	0.02
M038134	1850	0.9359(2)	21.71(18)	1928	0.9359(2)	22.21(19)	22.11	0.10
M038136	1900	0.9376(2)	21.66(18)	1982	0.9369(2)	22.18(19)	22.15	0.03
M038138	1800	0.9354(3)	21.50(18)	1874	0.9365(3)	21.97(19)	21.68	0.29
M038140	1700	0.9337(3)	21.25(17)	1766	0.9344(2)	21.68(18)	21.64	0.04
M038142	1600	0.9318(2)	21.05(17)	1660	0.9332(3)	21.43(17)	21.39	0.04
M038144	1500	0.9300(2)	20.84(16)	1553	0.9321(3)	21.18(16)	21.14	0.04
M038146	1900	0.9379(3)	21.59(18)	1981	0.9374(2)	22.11(19)	22.04	0.07
M038148	1950	0.9397(2)	21.50(18)	2035	0.9387(2)	22.05(18)	22.00	0.05
M038150	2000	0.9412(2)	21.48(18)	2089	0.9398(2)	22.05(18)	22.00	0.05
M038154	1900	0.9433(2)	20.39(16)	1979	0.9421(3)	20.90(17)	20.88	0.01
M038156	1800	0.9408(3)	20.29(17)	1872	0.9410(3)	20.75(18)	20.59	0.16
M087012	1600	0.9341(1)	20.53(15)	1659	0.9326(2)	20.90(16)	21.54	-0.64
M087016	300	0.9072(1)	19.26(5)	305	0.9177(1)	19.28(5)	19.20	0.09
M087019	1100	0.9203(1)	20.63(13)	1131	0.9250(1)	20.83(13)	20.89	-0.06
M087021	1300	0.9234(1)	21.13(14)	1342	0.9270(2)	21.40(15)	21.40	0.00
M087023	1500	0.9272(1)	21.48(16)	1554	0.9295(1)	21.83(16)	21.82	0.01
M087025	1600	0.9295(2)	21.59(17)	1659	0.9311(2)	21.98(18)	21.94	0.03
M087027	1700	0.9326(2)	21.51(17)	1767	0.9330(1)	21.94(18)	22.00	-0.06
M087029	1800	0.9365(2)	21.25(17)	1873	0.9362(2)	21.72(18)	21.77	-0.05
M087032	1900	0.9404(3)	21.01(18)	1980	0.9393(2)	21.53(19)	21.55	-0.02
M087033	1800	0.9389(1)	20.71(16)	1872	0.9377(2)	21.17(17)	21.38	-0.21

M087035	1700	0.9370(1)	20.51(16)	1765	0.9367(2)	20.93(16)	21.06	-0.14
M087037	1600	0.9349(1)	20.35(15)	1658	0.9355(1)	20.72(16)	20.83	-0.10
M087039	1500	0.9327(1)	20.20(15)	1552	0.9342(2)	20.53(15)	20.60	-0.07
M087041	1400	0.9308(1)	20.01(14)	1446	0.9329(1)	20.30(14)	20.39	-0.09
M087043	1300	0.9290(1)	19.79(13)	1340	0.9317(2)	20.05(14)	20.17	-0.12
M087045	1200	0.9270(1)	19.63(12)	1235	0.9306(1)	19.85(13)	19.92	-0.07
M087047	1100	0.9251(2)	19.46(13)	1130	0.9290(5)	19.65(13)	19.81	-0.16
M087049	1000	0.9234(1)	19.24(11)	1026	0.9282(1)	19.41(11)	19.49	-0.09
M087051	900	0.9217(2)	19.04(11)	922	0.9271(1)	19.17(11)	19.27	-0.10
M087053	800	0.9197(1)	18.90(9)	818	0.9262(1)	19.01(9)	19.04	-0.02
M087055	700	0.9180(2)	18.72(10)	715	0.9250(1)	18.81(10)	18.86	-0.06
M087057	600	0.9164(1)	18.50(8)	612	0.9240(2)	18.57(8)	18.65	-0.08
M087059	500	0.9147(1)	18.35(7)	509	0.9231(1)	18.40(7)	18.46	-0.06
M087061	400	0.9133(2)	18.18(7)	407	0.9223(2)	18.22(7)	18.25	-0.03
M087063	305	0.9123(0)	17.97(4)	310	0.9219(2)	17.99(4)	18.00	-0.01
M087065	302	0.9108(2)	18.34(6)	307	0.9212(2)	18.36(6)	18.19	0.18
M087067	302	0.9099(1)	18.56(5)	307	0.9201(2)	18.59(5)	18.51	0.07
M087069	500	0.9128(1)	18.84(7)	509	0.9211(2)	18.90(7)	19.02	-0.12
M087071	700	0.9156(1)	19.32(9)	715	0.9227(1)	19.41(9)	19.49	-0.09
M087073	900	0.9188(1)	19.73(10)	922	0.9246(2)	19.87(10)	19.98	-0.11
M087075	304	0.9096(1)	18.65(6)	309	0.9194(2)	18.67(6)	18.72	-0.04
M087077	300	0.9044(2)	20.01(7)	305	0.9148(2)	20.03(8)	20.06	-0.03
M087083	700	0.9054(1)	21.95(10)	716	0.9136(2)	22.05(10)	22.14	-0.10
M087085	1100	0.9124(1)	22.60(14)	1133	0.9173(2)	22.81(14)	23.05	-0.24

M087087	1300	0.9161(2)	22.94(16)	1344	0.9198(1)	23.22(17)	23.37	-0.15
M087089	1400	0.9179(2)	23.13(17)	1450	0.9209(2)	23.45(18)	23.59	-0.14
M087091	1500	0.9198(1)	23.29(17)	1556	0.9221(1)	23.65(18)	23.79	-0.13
M087093	1300	0.9155(1)	23.09(16)	1344	0.9196(2)	23.37(16)	23.44	-0.07
M087096	1100	0.9121(1)	22.69(14)	1133	0.9177(1)	22.90(14)	22.94	-0.04
M087098	900	0.9084(1)	22.37(12)	924	0.9154(2)	22.52(13)	22.57	-0.05
M087100	700	0.9052(1)	22.01(10)	716	0.9135(2)	22.11(10)	22.16	-0.05
M087102	500	0.9021(1)	21.66(7)	510	0.9116(2)	21.71(8)	21.82	-0.10
M087104	300	0.8995(1)	21.33(6)	306	0.9106(2)	21.35(6)	21.33	0.02
M087106	1500	0.9198(2)	23.30(18)	1556	0.9223(1)	23.66(18)	23.74	-0.08
M087109	1500	0.9222(3)	22.70(18)	1556	0.9253(1)	23.05(19)	22.93	0.12
M087111	1700	0.9265(1)	22.95(18)	1769	0.9278(2)	23.40(19)	23.36	0.04
M087113	1700	0.9277(1)	22.67(18)	1769	0.9290(1)	23.11(18)	23.04	0.07
M087115	1700	0.9288(1)	22.39(17)	1768	0.9299(1)	22.83(18)	22.80	0.03
M087117	1800	0.9312(2)	22.47(18)	1876	0.9314(1)	22.96(19)	22.96	-0.01
M087119	1900	0.9341(1)	22.44(18)	1983	0.9342(1)	22.98(19)	22.82	0.15
M087121	1700	0.9308(1)	21.93(17)	1768	0.9317(1)	22.36(18)	22.34	0.02
M087123	1500	0.9267(1)	21.62(16)	1554	0.9295(2)	21.97(16)	21.82	0.14
M087125	1300	0.9228(1)	21.28(14)	1342	0.9271(1)	21.54(15)	21.38	0.16
M087127	1100	0.9195(1)	20.83(13)	1132	0.9248(1)	21.03(13)	20.93	0.10
M087129	900	0.9160(1)	20.44(11)	923	0.9228(1)	20.58(11)	20.48	0.11
M087131	700	0.9125(1)	20.10(9)	715	0.9210(1)	20.19(9)	19.99	0.20
M087133	500	0.9095(2)	19.68(8)	510	0.9195(1)	19.74(8)	19.49	0.25
M087135	300	0.9072(1)	19.26(5)	305	0.9182(1)	19.29(5)	19.07	0.22

M087137	1700	0.9331(1)	21.39(16)	1767	0.9338(2)	21.82(17)	21.80	0.02
M087139	1700	0.9363(1)	20.67(16)	1765	0.9369(2)	21.09(16)	21.03	0.06
M087141	1700	0.9397(1)	19.90(15)	1764	0.9392(2)	20.31(16)	20.46	-0.15
M087143	1500	0.9356(1)	19.55(14)	1551	0.9365(1)	19.88(14)	20.02	-0.14
M087153	1800	0.9354(3)	21.51(19)	1874	0.9348(3)	21.98(19)	22.11	-0.13
M087155	1900	0.9375(2)	21.66(18)	1982	0.9365(2)	22.18(18)	22.25	-0.07
M087158	1500	0.9327(1)	20.20(15)	1552	0.9344(2)	20.53(15)	20.55	-0.02
M087160	1500	0.9367(3)	19.30(16)	1551	0.9383(1)	19.62(16)	19.57	0.05
M087162	1500	0.9398(1)	18.61(13)	1550	0.9409(1)	18.92(14)	18.93	-0.01
M087164	1300	0.9362(2)	18.14(12)	1338	0.9380(2)	18.38(13)	18.56	-0.17
M087166	1100	0.9325(1)	17.72(11)	1129	0.9361(2)	17.90(11)	17.96	-0.06
M087168	900	0.9285(2)	17.40(10)	921	0.9339(2)	17.53(10)	17.47	0.06
M087170	700	0.9255(1)	16.88(7)	714	0.9320(2)	16.97(7)	16.96	0.01
M087172	500	0.9222(1)	16.50(6)	509	0.9301(1)	16.55(6)	16.51	0.04
M087174	300	0.9197(0)	16.09(4)	305	0.9287(1)	16.11(4)	16.09	0.02
M087176	1100	0.9400(2)	16.04(10)	1127	0.9434(2)	16.21(11)	16.12	0.09
M087178	900	0.9363(2)	15.60(10)	919	0.9414(2)	15.72(10)	15.56	0.16
M087180	700	0.9333(1)	15.07(7)	713	0.9392(2)	15.15(7)	15.08	0.08
M087182	500	0.9293(1)	14.82(6)	508	0.9377(1)	14.86(6)	14.51	0.36
M087184	300	0.9256(3)	14.64(9)	304	0.9360(2)	14.66(9)	14.11	0.55
M092019	1700	0.9329(1)	21.44(17)	1767	0.9328(4)	21.87(17)	22.07	-0.20
M092021	1800	0.9364(2)	21.28(17)	1873	0.9367(3)	21.75(18)	21.65	0.10
M092023	1900	0.9402(2)	21.06(17)	1980	0.9397(3)	21.57(18)	21.48	0.10
M092025	2000	0.9433(4)	21.01(19)	2088	0.9424(3)	21.57(20)	21.39	0.19

M092028	1900	0.9418(2)	20.72(17)	1980	0.9409(4)	21.23(18)	21.17	0.06
M092030	1900	0.9424(2)	20.57(17)	1979	0.9402(4)	21.08(18)	21.35	-0.27
M092032	1900	0.9432(2)	20.40(17)	1979	0.9412(6)	20.91(17)	21.09	-0.19
M092034	1900	0.9446(1)	20.11(16)	1978	0.9420(5)	20.61(17)	20.91	-0.30
M092036	1900	0.9456(3)	19.87(17)	1978	0.9429(5)	20.37(17)	20.68	-0.31
M092038	1900	0.9467(1)	19.64(15)	1977	0.9443(4)	20.13(16)	20.36	-0.23

565

Table S4. *P*-*V*-*T* data of bridgmanite. . The initial data is from Katsura et al. [2009c] and Tange et al. [2012], and the pressure and tempeatures are recalcuted in this study.

Data #	T before correction (K)	V/V_0^{MgO}	P^{MgO} before correction (GPa)	T after correction (K)	V/V_0^{Brg}	P^{MgO} after correction (GPa)	P^{Brg} (GPa)	P^{MgO}-P^{Brg} (GPa)
M1	1300	0.8891(1)	30.25(21)	1351	0.9254(7)	30.58(22)	30.28	0.30
M1	1100	0.8854(1)	30.07(18)	1139	0.9215(9)	30.31(19)	30.18	0.14
M1	900	0.8829(1)	29.54(15)	928	0.9184(9)	29.72(16)	29.84	-0.13
M1	700	0.8810(3)	28.87(15)	719	0.9162(9)	28.98(15)	29.26	-0.28
M1	500	0.8780(1)	28.60(10)	512	0.9141(6)	28.67(11)	28.80	-0.13
M1	300	0.8769(0)	27.91(6)	306	0.9131(4)	27.94(7)	28.14	-0.20
M2	1500	0.8548(4)	42.56(35)	1577	0.8987(4)	43.06(36)	42.53	0.53
M2	1300	0.8529(3)	41.91(29)	1360	0.8967(4)	42.30(30)	41.80	0.50
M2	1100	0.8513(2)	41.17(23)	1145	0.8941(5)	41.47(24)	41.41	0.06
M2	900	0.8486(3)	40.86(22)	933	0.8920(4)	41.07(22)	40.84	0.22
M2	700	0.8470(1)	40.21(16)	722	0.8899(5)	40.34(16)	40.34	0.00
M2	500	0.8454(1)	39.58(12)	514	0.8886(4)	39.66(12)	39.67	-0.01
M2	300	0.8443(4)	38.96(19)	308	0.8877(5)	39.00(19)	39.05	-0.05
M3	1500	0.8297(3)	52.00(36)	1584	0.8771(3)	52.56(38)	52.29	0.28
M3	1300	0.8277(3)	51.48(31)	1365	0.8753(4)	51.92(33)	51.58	0.34
M3	1100	0.8259(3)	50.94(27)	1149	0.8731(4)	51.26(28)	51.14	0.12
M3	900	0.8239(3)	50.47(23)	936	0.8712(5)	50.70(23)	50.62	0.08
M3	700	0.8218(5)	50.04(29)	724	0.8695(5)	50.19(30)	50.05	0.13
M3	500	0.8206(5)	49.35(28)	515	0.8682(4)	49.43(28)	49.48	-0.04

M3	300	0.8198(4)	48.67(20)	308	0.8673(3)	48.71(20)	48.97	-0.26
M4	1500	0.8067(3)	61.93(37)	1590	0.8581(7)	62.54(39)	61.89	0.64
M4	1300	0.8030(4)	62.32(35)	1371	0.8548(7)	62.80(37)	62.13	0.66
M4	1100	0.8003(8)	62.24(49)	1154	0.8527(6)	62.60(50)	61.77	0.83
M4	900	0.7987(7)	61.68(40)	939	0.8507(8)	61.94(41)	61.41	0.53
M4	700	0.7965(7)	61.43(38)	727	0.8487(12)	61.60(39)	61.17	0.43
M4	500	0.7952(7)	60.87(38)	517	0.8472(10)	60.97(38)	60.74	0.23
M4	300	0.7937(7)	60.58(38)	309	0.8461(10)	60.62(38)	60.46	0.16
M252031	1900	0.9313(1)	23.09(19)	1985	0.9614(1)	23.63(20)	23.05	0.57
M252029	1800	0.9283(0)	23.15(18)	1877	0.9583(1)	23.64(19)	23.16	0.48
M252027	1700	0.9253(0)	23.24(18)	1770	0.9551(1)	23.69(19)	23.31	0.37
M252034	1700	0.9270(1)	22.82(18)	1769	0.9559(1)	23.26(19)	23.06	0.20
M252025	1600	0.9226(1)	23.24(18)	1663	0.9522(1)	23.64(18)	23.44	0.21
M252023	1500	0.9195(2)	23.36(18)	1556	0.9489(1)	23.72(18)	23.66	0.06
M252036	1500	0.9235(1)	22.39(16)	1555	0.9523(1)	22.74(17)	22.58	0.16
M252038	1300	0.9203(1)	21.90(15)	1343	0.9490(1)	22.17(15)	22.02	0.16
M252040	1100	0.9167(1)	21.51(13)	1132	0.9458(1)	21.72(13)	21.52	0.20
M252042	900	0.9142(1)	20.90(11)	923	0.9429(1)	21.04(11)	20.96	0.08
M252044	700	0.9113(1)	20.42(9)	716	0.9402(1)	20.51(9)	20.43	0.08
M252046	500	0.9086(1)	19.93(7)	510	0.9378(1)	19.99(7)	19.91	0.08
M252048	306	0.9064(1)	19.50(5)	311	0.9358(1)	19.52(5)	19.56	-0.03
M252050	300	0.9076(1)	19.15(5)	305	0.9385(1)	19.18(5)	18.59	0.58
M253054	2500	0.9160(1)	30.69(31)	2661	0.9480(1)	31.74(33)	32.43	-0.70
M253052	2300	0.9127(1)	30.23(29)	2437	0.9455(1)	31.12(31)	31.53	-0.41

M253050	2100	0.9096(1)	29.75(28)	2216	0.9432(1)	30.50(29)	30.56	-0.06
M253032	1900	0.9071(0)	29.11(25)	1996	0.9402(1)	29.73(27)	29.91	-0.19
M253013	1900	0.9173(1)	26.46(22)	1991	0.9482(1)	27.05(24)	27.22	-0.17
M253034	1700	0.9046(1)	28.49(23)	1778	0.9380(1)	29.00(25)	28.99	0.01
M253015	1700	0.9144(1)	25.94(21)	1774	0.9462(1)	26.41(22)	26.22	0.19
M253036	1500	0.9028(1)	27.70(21)	1562	0.9359(1)	28.10(22)	28.08	0.02
M253017	1500	0.9124(1)	25.17(19)	1559	0.9438(1)	25.55(20)	25.36	0.19
M253038	1300	0.9001(1)	27.15(19)	1348	0.9335(1)	27.46(19)	27.32	0.14
M253019	1300	0.9095(1)	24.62(17)	1346	0.9414(1)	24.91(18)	24.59	0.32
M253040	1100	0.8982(1)	26.40(16)	1136	0.9311(1)	26.63(17)	26.64	-0.01
M253021	1100	0.9074(1)	23.91(14)	1134	0.9388(1)	24.12(15)	23.90	0.23
M253042	900	0.8953(1)	25.93(14)	926	0.9287(1)	26.09(14)	25.98	0.11
M253023	900	0.9044(1)	23.44(12)	925	0.9363(1)	23.59(13)	23.23	0.37
M253044	700	0.8934(1)	25.25(11)	718	0.9263(1)	25.36(11)	25.41	-0.05
M253025	700	0.9023(1)	22.79(10)	717	0.9340(1)	22.89(10)	22.58	0.30
M253046	500	0.8904(1)	24.93(9)	511	0.9243(1)	24.99(9)	24.84	0.15
M253027	500	0.8993(1)	22.41(8)	510	0.9314(1)	22.47(8)	22.19	0.28
M253031	300	0.8886(1)	24.41(7)	306	0.9234(1)	24.44(7)	24.11	0.33
M253048	300	0.8890(1)	24.28(7)	306	0.9229(1)	24.31(7)	24.29	0.02
M253029	300	0.8978(1)	21.81(6)	306	0.9297(1)	21.84(6)	21.74	0.09
M253059	300	1.0000(0)	0.00(0)	300	1.0000(1)	0.00(0)	0.00	0.00
M526017	1600	0.9015(5)	28.70(27)	1670	0.9368(3)	29.15(28)	28.59	0.56
M526020	1700	0.8998(5)	29.81(30)	1780	0.9358(3)	30.33(31)	29.78	0.55
M526021	1800	0.9033(6)	29.50(31)	1888	0.9369(3)	30.07(32)	30.20	-0.13

M526024	1900	0.9021(5)	30.46(32)	1998	0.9379(3)	31.09(33)	30.68	0.41
M526025	1700	0.9013(6)	29.39(31)	1779	0.9348(3)	29.90(32)	30.10	-0.20
M526028	1500	0.8975(6)	29.15(29)	1564	0.9311(4)	29.56(30)	29.79	-0.23
M526029	1300	0.8946(6)	28.68(27)	1350	0.9280(4)	29.00(27)	29.34	-0.33
M526032	1100	0.8919(5)	28.16(25)	1137	0.9251(3)	28.40(25)	28.81	-0.41
M526033	900	0.8894(6)	27.63(24)	927	0.9221(3)	27.80(24)	28.43	-0.63
M526045	1700	0.8812(7)	35.21(38)	1787	0.9170(4)	35.78(40)	36.67	-0.90
M526046	1800	0.8808(5)	35.98(36)	1897	0.9176(4)	36.61(38)	37.27	-0.66
M526047	1700	0.8796(5)	35.71(35)	1787	0.9160(4)	36.28(37)	37.08	-0.80
M526048	1500	0.8771(5)	35.17(33)	1570	0.9131(4)	35.63(34)	36.57	-0.94
M526049	1300	0.8745(5)	34.69(31)	1355	0.9101(4)	35.04(31)	36.19	-1.14
M526050	1100	0.8719(5)	34.23(28)	1141	0.9073(4)	34.49(29)	35.79	-1.30
M526051	900	0.8694(5)	33.73(26)	930	0.9050(4)	33.92(26)	35.23	-1.31
M526052	700	0.8671(5)	33.25(24)	720	0.9026(4)	33.37(24)	34.82	-1.45
M554011	1700	0.9211(4)	24.25(22)	1772	0.9513(4)	24.71(23)	24.55	0.16
M554012	1700	0.9191(3)	24.74(21)	1772	0.9497(3)	25.21(22)	25.07	0.13
M554013	1500	0.9150(4)	24.49(21)	1558	0.9457(4)	24.87(22)	24.73	0.14
M554014	1300	0.9116(5)	24.07(21)	1345	0.9435(4)	24.36(22)	23.86	0.50
M554015	1100	0.9085(4)	23.61(19)	1134	0.9398(4)	23.82(20)	23.56	0.26
M554016	900	0.9055(4)	23.14(18)	924	0.9368(4)	23.29(18)	23.06	0.24
M554017	700	0.9030(4)	22.59(16)	716	0.9342(4)	22.69(16)	22.53	0.17
M554018	500	0.9005(4)	22.09(15)	510	0.9316(4)	22.15(15)	22.14	0.01
M554019	304	0.8979(3)	21.78(11)	310	0.9292(3)	21.81(11)	21.94	-0.13
M554021	1700	0.9176(5)	25.12(25)	1773	0.9486(4)	25.59(26)	25.41	0.18

M554022	1700	0.9172(5)	25.21(25)	1773	0.9482(4)	25.68(25)	25.55	0.13
M554023	1800	0.9188(5)	25.45(25)	1881	0.9490(4)	25.98(26)	26.11	-0.14
M554024	1800	0.9189(5)	25.44(25)	1881	0.9502(5)	25.96(26)	25.74	0.22
M554025	1900	0.9220(5)	25.33(26)	1989	0.9515(3)	25.90(27)	26.15	-0.25
M557019	1900	0.8685(5)	40.52(41)	2013	0.9087(5)	41.27(43)	41.62	-0.35
M554020	1700	0.8658(5)	40.09(38)	1792	0.9065(4)	40.70(40)	40.88	-0.18
M554021	1500	0.8638(5)	39.45(34)	1574	0.9043(4)	39.94(35)	40.17	-0.24
M645023	1700	0.8302(5)	53.15(44)	1805	0.8778(5)	53.85(47)	53.55	0.30
M645024	1500	0.8270(4)	53.11(39)	1584	0.8736(5)	53.68(41)	54.00	-0.32
M645025	1300	0.8250(4)	52.62(35)	1366	0.8719(4)	53.06(36)	53.26	-0.20
M645026	1100	0.8233(4)	51.98(31)	1150	0.8704(4)	52.31(32)	52.50	-0.19
M645027	900	0.8221(4)	51.20(27)	936	0.8692(4)	51.44(28)	51.63	-0.19
M645028	700	0.8207(4)	50.53(24)	725	0.8679(4)	50.69(24)	50.89	-0.20
M645029	500	0.8194(4)	49.86(21)	515	0.8664(4)	49.94(21)	50.38	-0.43
M645030	304	0.8184(4)	49.29(21)	312	0.8658(3)	49.32(21)	49.75	-0.42
M654032	1900	0.8303(5)	54.45(49)	2029	0.8781(3)	55.32(52)	55.02	0.30
M659028	1700	0.8508(5)	45.29(41)	1798	0.8947(3)	45.94(43)	45.85	0.09
M659029	1500	0.8486(4)	44.77(35)	1578	0.8933(3)	45.28(37)	44.85	0.44
M659030	1300	0.8470(4)	44.04(32)	1361	0.8907(3)	44.44(33)	44.42	0.02
M659031	1100	0.8444(4)	43.70(28)	1146	0.8880(3)	44.00(29)	44.10	-0.10
M659032	900	0.8432(4)	42.85(26)	933	0.8866(3)	43.07(27)	43.27	-0.21
M659033	700	0.8417(4)	42.14(22)	723	0.8850(3)	42.28(22)	42.61	-0.33
M659034	500	0.8401(4)	41.55(19)	514	0.8834(2)	41.64(19)	42.07	-0.43
M659035	308	0.8389(4)	41.06(18)	316	0.8821(2)	41.09(18)	41.71	-0.61

M659036	1700	0.8501(4)	45.54(40)		1798	0.8943(3)	46.19(42)	46.02	0.18
M697010	305	0.8724(5)	29.35(19)		312	0.9104(2)	29.38(19)	29.25	0.14

Original data labeled as ‘M1’, ‘M2’, ‘M3, and ‘M4’ are from Tange *et al.* [2014]. The other data are from Katsura *et al.* [2009c].

Table S5. Thermoelastic paremeters of the adiabatic mantle

Depth (km)	ρ (kg m^{-3})#	g (m s^{-2}) #	P (GPa) #	T (K)	dT/dP (K GPa^{-1})	dT/dP (K GPa^{-1})	α (K^{-1})	Cp (J kg^{-1})	Cp (kJ m^{-3})	Cv/3nR	V/V_0	γ	1+αγT	K_T (GPa)	K_T (GPa)
50	3127(4)	9.85	1.46	1616(17)	15.9(9)	0.530(29)	4.02(23)	1305(5)	4079(10)	0.981(1)	1.032(1)	1.102(4)	1.072(4)	102.5(4)	109.8(6)
60	3136(4)	9.85	1.79	1622(17)	15.7(8)	0.521(27)	3.95(21)	1303(4)	4086(9)	0.981(1)	1.029(1)	1.094(3)	1.070(4)	103.9(4)	111.2(6)
70	3145(4)	9.86	2.12	1627(17)	15.4(8)	0.512(25)	3.87(20)	1301(4)	4093(8)	0.981(1)	1.026(1)	1.086(3)	1.068(4)	105.3(4)	112.5(6)
80	3155(3)	9.86	2.45	1632(17)	15.1(7)	0.504(24)	3.80(18)	1300(4)	4100(8)	0.982(1)	1.023(1)	1.077(3)	1.067(3)	106.7(4)	113.8(6)
90	3164(3)	9.86	2.79	1637(17)	14.9(7)	0.495(22)	3.74(17)	1298(4)	4108(7)	0.982(1)	1.020(1)	1.069(3)	1.065(3)	108.1(4)	115.2(5)
100	3173(3)	9.87	3.12	1642(17)	14.6(6)	0.487(21)	3.67(16)	1297(3)	4115(7)	0.982(1)	1.017(1)	1.062(3)	1.064(3)	109.5(4)	116.5(5)
110	3182(3)	9.87	3.45	1646(17)	14.4(6)	0.480(20)	3.61(15)	1296(3)	4122(6)	0.982(1)	1.014(1)	1.054(3)	1.063(3)	110.9(4)	117.8(5)
120	3191(3)	9.87	3.78	1651(17)	14.2(6)	0.472(18)	3.55(14)	1294(3)	4129(6)	0.983(1)	1.011(1)	1.046(2)	1.061(3)	112.3(4)	119.2(5)
130	3199(3)	9.87	4.12	1656(17)	14.0(5)	0.465(17)	3.49(13)	1293(3)	4137(5)	0.983(1)	1.009(1)	1.039(2)	1.060(2)	113.7(4)	120.5(5)
140	3208(3)	9.88	4.45	1660(17)	13.8(5)	0.457(16)	3.43(12)	1292(3)	4144(5)	0.983(1)	1.006(1)	1.032(2)	1.059(2)	115.0(4)	121.8(5)
150	3217(3)	9.88	4.78	1665(17)	13.5(5)	0.450(15)	3.38(11)	1291(3)	4151(5)	0.983(1)	1.003(1)	1.025(2)	1.058(2)	116.4(4)	123.1(5)
160	3225(3)	9.88	5.12	1669(17)	13.3(4)	0.444(15)	3.32(11)	1289(2)	4159(5)	0.983(1)	1.001(1)	1.018(2)	1.056(2)	117.8(4)	124.4(4)
170	3234(3)	9.89	5.45	1674(17)	13.1(4)	0.437(14)	3.27(10)	1288(2)	4166(4)	0.984(1)	0.998(1)	1.011(2)	1.055(2)	119.2(4)	125.8(4)
180	3242(3)	9.89	5.78	1678(17)	12.9(4)	0.431(13)	3.22(10)	1287(2)	4173(4)	0.984(1)	0.995(1)	1.004(2)	1.054(2)	120.5(4)	127.1(4)
190	3251(2)	9.89	6.11	1682(17)	12.8(4)	0.425(13)	3.17(9)	1286(2)	4181(4)	0.984(1)	0.993(1)	0.997(2)	1.053(2)	121.9(4)	128.4(4)
200	3259(2)	9.89	6.45	1686(17)	12.6(4)	0.420(12)	3.12(9)	1285(2)	4188(4)	0.984(1)	0.990(1)	0.991(2)	1.052(2)	123.3(4)	129.7(4)
210	3267(2)	9.90	6.78	1690(17)	12.4(3)	0.416(12)	3.08(8)	1284(2)	4195(4)	0.984(1)	0.988(1)	0.984(2)	1.051(2)	124.6(4)	131.0(4)
220	3275(2)	9.90	7.11	1695(17)	12.2(3)	0.411(11)	3.03(8)	1283(2)	4203(4)	0.984(1)	0.985(1)	0.978(2)	1.050(1)	126.0(4)	132.3(4)
230	3284(2)	9.90	7.45	1699(18)	12.1(3)	0.407(11)	2.99(8)	1282(2)	4210(4)	0.985(1)	0.983(1)	0.972(2)	1.049(1)	127.4(4)	133.6(4)
240	3292(2)	9.91	7.79	1703(18)	11.9(3)	0.403(11)	2.94(8)	1281(2)	4218(5)	0.985(1)	0.980(1)	0.965(2)	1.048(1)	128.7(4)	135.0(4)
250	3300(2)	9.91	8.14	1707(18)	11.7(3)	0.400(11)	2.90(7)	1280(2)	4225(5)	0.985(1)	0.978(1)	0.959(2)	1.047(1)	130.1(4)	136.3(4)
260	3308(2)	9.92	8.48	1711(18)	11.6(3)	0.396(11)	2.86(7)	1279(2)	4233(5)	0.985(1)	0.975(1)	0.953(2)	1.047(1)	131.5(4)	137.6(4)
270	3316(2)	9.92	8.82	1715(18)	11.4(3)	0.392(11)	2.82(7)	1279(2)	4240(5)	0.985(1)	0.973(1)	0.947(2)	1.046(1)	132.9(4)	139.0(4)
280	3324(2)	9.93	9.17	1718(18)	11.2(3)	0.388(11)	2.78(7)	1278(2)	4248(5)	0.985(1)	0.971(1)	0.941(2)	1.045(1)	134.3(4)	140.3(4)
290	3332(2)	9.94	9.51	1722(18)	11.1(3)	0.383(11)	2.74(7)	1277(2)	4255(6)	0.985(1)	0.968(1)	0.935(2)	1.044(1)	135.7(4)	141.7(4)
300	3340(2)	9.94	9.86	1726(18)	10.9(3)	0.379(11)	2.70(7)	1276(2)	4263(6)	0.985(1)	0.966(1)	0.929(2)	1.043(1)	137.0(4)	143.0(4)
310	3348(2)	9.95	10.20	1730(18)	10.8(3)	0.375(11)	2.67(8)	1275(2)	4270(6)	0.986(1)	0.964(1)	0.924(2)	1.043(1)	138.4(4)	144.3(4)

320	3356(2)	9.95	10.55	1734(18)	10.7(3)	0.371(11)	2.63(8)	1275(3)	4278(6)	0.986(1)	0.961(1)	0.918(2)	1.042(1)	139.8(4)	145.7(4)
330	3364(2)	9.95	10.90	1737(18)	10.5(3)	0.367(11)	2.60(8)	1274(3)	4285(7)	0.986(1)	0.959(1)	0.913(2)	1.041(1)	141.2(4)	147.0(4)
340	3372(2)	9.95	11.25	1741(18)	10.4(3)	0.362(11)	2.56(8)	1273(3)	4293(7)	0.986(1)	0.957(1)	0.907(2)	1.040(1)	142.6(4)	148.4(4)
350	3380(2)	9.95	11.60	1744(18)	10.3(3)	0.358(12)	2.53(8)	1272(3)	4300(7)	0.986(1)	0.955(1)	0.902(2)	1.040(1)	144.0(4)	149.7(4)
360	3388(2)	9.95	11.95	1748(18)	10.1(3)	0.355(12)	2.49(8)	1272(3)	4308(7)	0.986(1)	0.953(1)	0.897(2)	1.039(1)	145.3(4)	151.0(4)
370	3395(2)	9.96	12.30	1751(18)	10.0(3)	0.351(12)	2.46(8)	1271(3)	4315(8)	0.986(1)	0.950(1)	0.891(2)	1.038(1)	146.7(4)	152.4(4)
380	3403(2)	9.96	12.65	1755(18)	9.9(4)	0.347(12)	2.43(9)	1270(3)	4323(8)	0.986(1)	0.948(1)	0.886(2)	1.038(1)	148.1(4)	153.7(4)
390	3411(3)	9.97	13.00	1758(18)	9.7(4)	0.344(13)	2.40(9)	1270(3)	4330(8)	0.986(1)	0.946(1)	0.881(2)	1.037(1)	149.5(4)	155.1(4)
400	3418(3)	9.97	13.35	1762(18)	9.6(4)	0.340(13)	2.37(9)	1269(3)	4338(8)	0.986(1)	0.944(1)	0.876(2)	1.037(1)	150.9(4)	156.4(4)
410	3426(3)	9.97	13.73	1765(18)	9.5(4)	0.354(14)	2.34(9)	1268(3)	4346(9)	0.987(1)	0.942(1)	0.871(2)	1.036(2)	152.4(4)	157.8(4)
410	3606(3)	9.97	13.73	1825(18)	9.6(5)	0.357(17)	2.42(12)	1282(2)	4623(5)	0.992(1)	0.963(1)	0.927(1)	1.041(2)	193.0(3)	200.9(4)
420	3613(2)	9.97	14.10	1829(18)	9.5(4)	0.355(16)	2.40(11)	1281(2)	4630(5)	0.992(1)	0.961(1)	0.925(1)	1.041(2)	194.3(3)	202.2(4)
430	3620(2)	9.98	14.48	1833(18)	9.4(4)	0.353(15)	2.38(10)	1281(2)	4636(5)	0.992(1)	0.959(1)	0.922(1)	1.040(2)	195.6(3)	203.5(4)
440	3626(2)	9.98	14.85	1836(18)	9.3(4)	0.352(15)	2.36(9)	1280(2)	4643(5)	0.992(1)	0.958(1)	0.919(1)	1.040(2)	196.9(3)	204.7(4)
450	3633(2)	9.98	15.23	1840(18)	9.3(4)	0.350(14)	2.34(9)	1280(2)	4650(5)	0.992(1)	0.956(1)	0.917(1)	1.039(2)	198.1(3)	206.0(3)
460	3639(2)	9.98	15.61	1843(18)	9.2(3)	0.348(13)	2.32(8)	1279(2)	4656(5)	0.992(1)	0.954(1)	0.914(1)	1.039(1)	199.4(3)	207.2(3)
470	3646(2)	9.98	15.99	1847(18)	9.1(3)	0.347(12)	2.30(7)	1279(2)	4663(5)	0.992(2)	0.953(1)	0.912(1)	1.039(1)	200.7(3)	208.5(3)
480	3652(2)	9.99	16.37	1850(18)	9.0(3)	0.345(11)	2.28(7)	1279(2)	4670(6)	0.992(2)	0.951(1)	0.909(1)	1.038(1)	202.0(3)	209.8(3)
490	3659(2)	9.99	16.75	1854(18)	9.0(3)	0.344(11)	2.26(6)	1278(2)	4677(6)	0.992(2)	0.949(1)	0.906(1)	1.038(1)	203.3(3)	211.1(3)
500	3665(2)	9.99	17.13	1857(18)	8.9(3)	0.342(10)	2.24(6)	1278(2)	4683(7)	0.992(2)	0.948(0)	0.904(1)	1.038(1)	204.6(3)	212.3(3)
510	3672(2)	9.99	17.52	1860(18)	8.8(2)	0.341(10)	2.23(6)	1277(2)	4690(7)	0.992(2)	0.946(0)	0.901(1)	1.037(1)	205.9(3)	213.6(3)
520	3678(2)	9.99	17.91	1864(18)	8.8(2)	0.339(9)	2.21(5)	1277(2)	4697(7)	0.992(2)	0.944(0)	0.899(1)	1.037(1)	207.2(3)	214.9(3)
520	3737(3)	9.99	17.91	1907(18)	10.1(5)	0.392(19)	2.56(12)	1290(3)	4822(6)	0.996(1)	0.953(1)	0.898(1)	1.044(2)	224.1(4)	233.9(5)
530	3743(3)	10.00	18.29	1911(18)	10.0(5)	0.389(18)	2.53(12)	1290(2)	4827(6)	0.996(1)	0.952(1)	0.895(1)	1.043(2)	225.7(4)	235.4(5)
540	3750(2)	10.00	18.68	1915(18)	9.9(4)	0.386(17)	2.50(11)	1289(2)	4832(5)	0.996(1)	0.950(1)	0.892(1)	1.043(2)	227.2(4)	236.9(5)
550	3756(2)	10.00	19.07	1919(18)	9.8(4)	0.383(17)	2.47(10)	1288(2)	4837(5)	0.996(1)	0.949(1)	0.888(1)	1.042(2)	228.8(4)	238.4(5)
560	3763(2)	10.00	19.46	1922(18)	9.7(4)	0.380(16)	2.44(10)	1287(2)	4842(4)	0.996(1)	0.947(1)	0.885(1)	1.042(2)	230.4(4)	239.9(5)
570	3769(2)	10.00	19.86	1926(18)	9.6(4)	0.377(15)	2.41(9)	1286(2)	4848(4)	0.995(1)	0.945(1)	0.882(1)	1.041(2)	232.0(4)	241.5(4)
580	3776(2)	10.00	20.25	1930(18)	9.5(4)	0.374(14)	2.38(9)	1285(2)	4853(4)	0.995(1)	0.944(1)	0.879(1)	1.040(2)	233.5(4)	243.0(4)
590	3782(2)	10.00	20.65	1934(18)	9.4(3)	0.372(13)	2.36(8)	1284(2)	4858(3)	0.995(1)	0.942(0)	0.877(1)	1.040(2)	235.1(4)	244.5(4)

600	3788(2)	10.00	21.04	1937(19)	9.3(3)	0.369(13)	2.33(7)	1284(1)	4863(3)	0.995(1)	0.940(0)	0.874(1)	1.039(1)	236.7(4)	246.0(4)
610	3795(2)	10.00	21.44	1941(19)	9.2(3)	0.365(12)	2.30(7)	1283(1)	4868(3)	0.995(1)	0.939(0)	0.871(1)	1.039(1)	238.3(4)	247.5(4)
620	3801(2)	10.01	21.84	1945(19)	9.1(3)	0.362(11)	2.28(6)	1282(1)	4874(3)	0.995(1)	0.937(0)	0.868(1)	1.038(1)	239.9(4)	249.1(4)
630	3807(2)	10.01	22.24	1948(19)	9.0(3)	0.358(11)	2.25(6)	1281(1)	4879(3)	0.995(1)	0.936(0)	0.865(1)	1.038(1)	241.4(4)	250.6(3)
640	3814(2)	10.01	22.64	1952(19)	8.9(3)	0.355(10)	2.22(5)	1281(1)	4884(3)	0.995(1)	0.934(0)	0.862(1)	1.037(1)	243.0(4)	252.1(3)
650	3820(2)	10.01	23.04	1955(19)	8.8(2)	0.351(9)	2.20(5)	1280(1)	4890(3)	0.995(1)	0.933(0)	0.859(1)	1.037(1)	244.6(4)	253.7(3)
660	3826(2)	10.01	23.44	1959(19)	8.7(2)	0.348(9)	2.17(5)	1279(1)	4895(3)	0.995(1)	0.931(0)	0.857(1)	1.036(1)	246.2(4)	255.2(3)
660	4286(3)	10.01	23.44	1925(19)	9.1(2)	0.363(9)	2.65(6)	1306(2)	5600(7)	1.007(1)	0.958(1)	0.872(2)	1.044(1)	302.7(5)	316.1(5)
670	4292(3)	10.01	23.84	1929(19)	9.1(2)	0.362(9)	2.63(6)	1306(2)	5605(7)	1.007(1)	0.957(1)	0.869(2)	1.044(1)	304.2(5)	317.6(5)
680	4298(3)	10.01	24.27	1932(19)	9.0(2)	0.395(9)	2.61(6)	1305(2)	5610(7)	1.007(1)	0.956(1)	0.865(2)	1.044(1)	305.8(5)	319.2(4)
690	4304(3)	10.01	24.71	1936(19)	9.0(2)	0.394(9)	2.60(5)	1305(2)	5616(6)	1.007(1)	0.954(1)	0.861(2)	1.043(1)	307.5(5)	320.8(4)
700	4310(3)	10.01	25.15	1940(19)	8.9(2)	0.392(9)	2.58(5)	1304(2)	5621(6)	1.007(1)	0.953(1)	0.857(2)	1.043(1)	309.1(5)	322.4(4)
710	4316(3)	10.01	25.59	1944(19)	8.9(2)	0.391(9)	2.56(5)	1304(2)	5627(6)	1.007(1)	0.952(1)	0.854(2)	1.043(1)	310.8(5)	324.0(4)
720	4322(3)	10.01	26.03	1948(19)	8.8(2)	0.389(9)	2.55(5)	1303(2)	5632(6)	1.007(1)	0.950(1)	0.850(2)	1.042(1)	312.4(5)	325.6(4)
730	4328(3)	10.01	26.48	1952(19)	8.8(2)	0.387(8)	2.53(5)	1303(2)	5638(6)	1.007(1)	0.949(1)	0.846(2)	1.042(1)	314.1(5)	327.2(4)
740	4333(2)	10.01	26.92	1956(19)	8.7(2)	0.386(8)	2.51(4)	1302(2)	5643(6)	1.006(1)	0.948(1)	0.843(2)	1.041(1)	315.8(5)	328.9(4)
750	4339(2)	10.00	27.36	1960(19)	8.7(2)	0.384(8)	2.50(4)	1302(2)	5649(6)	1.006(1)	0.947(1)	0.839(2)	1.041(1)	317.4(5)	330.5(4)
760	4345(2)	10.00	27.81	1963(19)	8.6(2)	0.383(8)	2.48(4)	1301(2)	5654(6)	1.006(1)	0.945(1)	0.836(1)	1.041(1)	319.1(5)	332.1(4)
770	4351(2)	10.00	28.25	1967(19)	8.6(2)	0.381(8)	2.47(4)	1301(2)	5659(6)	1.006(1)	0.944(1)	0.832(1)	1.040(1)	320.7(5)	333.7(4)
780	4357(2)	10.00	28.70	1971(19)	8.5(2)	0.380(8)	2.45(4)	1300(2)	5665(6)	1.006(1)	0.943(1)	0.829(1)	1.040(1)	322.4(5)	335.3(4)
790	4363(2)	10.00	29.14	1975(20)	8.5(2)	0.378(7)	2.44(4)	1300(2)	5670(6)	1.006(1)	0.941(1)	0.825(1)	1.040(1)	324.1(5)	336.9(4)
800	4369(2)	9.99	29.59	1979(20)	8.4(2)	0.376(7)	2.42(4)	1299(2)	5676(6)	1.006(1)	0.940(1)	0.822(1)	1.039(1)	325.7(5)	338.6(4)
810	4374(2)	9.99	30.04	1982(20)	8.4(2)	0.375(7)	2.41(3)	1299(2)	5681(6)	1.006(1)	0.939(1)	0.818(1)	1.039(1)	327.4(5)	340.2(4)
820	4380(2)	9.99	30.48	1986(20)	8.4(2)	0.373(7)	2.39(3)	1298(2)	5687(6)	1.006(1)	0.938(1)	0.815(1)	1.039(1)	329.1(5)	341.8(4)
830	4386(2)	9.99	30.93	1990(20)	8.3(2)	0.372(7)	2.38(3)	1298(2)	5692(6)	1.006(1)	0.936(1)	0.811(1)	1.038(1)	330.7(5)	343.4(4)
840	4392(2)	9.99	31.38	1994(20)	8.3(1)	0.371(7)	2.36(3)	1297(2)	5698(6)	1.006(1)	0.935(1)	0.808(1)	1.038(1)	332.4(5)	345.0(4)
850	4397(2)	9.98	31.82	1997(20)	8.2(1)	0.369(7)	2.35(3)	1297(2)	5703(6)	1.006(1)	0.934(1)	0.805(1)	1.038(1)	334.0(5)	346.6(4)
860	4403(2)	9.98	32.27	2001(20)	8.2(1)	0.368(6)	2.34(3)	1297(2)	5709(6)	1.006(1)	0.933(0)	0.801(1)	1.037(1)	335.7(5)	348.3(4)
870	4409(2)	9.98	32.72	2005(20)	8.1(1)	0.366(6)	2.32(3)	1296(2)	5714(6)	1.006(1)	0.932(0)	0.798(1)	1.037(1)	337.3(5)	349.9(4)
880	4414(2)	9.98	33.17	2008(20)	8.1(1)	0.365(6)	2.31(3)	1296(2)	5719(6)	1.006(1)	0.930(0)	0.795(1)	1.037(1)	339.0(5)	351.5(4)

890	4420(2)	9.98	33.62	2012(20)	8.1(1)	0.363(6)	2.30(3)	1295(2)	5725(6)	1.006(1)	0.929(0)	0.792(1)	1.037(1)	340.7(5)	353.1(4)
900	4426(2)	9.98	34.07	2016(20)	8.0(1)	0.362(6)	2.28(3)	1295(2)	5730(6)	1.006(1)	0.928(0)	0.788(1)	1.036(1)	342.3(5)	354.7(4)
910	4432(2)	9.98	34.53	2019(20)	8.0(1)	0.361(6)	2.27(3)	1294(2)	5736(7)	1.006(1)	0.927(0)	0.785(1)	1.036(1)	344.0(5)	356.4(4)
920	4437(2)	9.98	34.98	2023(20)	7.9(1)	0.359(6)	2.26(2)	1294(2)	5741(7)	1.006(1)	0.926(0)	0.782(1)	1.036(1)	345.7(5)	358.0(4)
930	4443(2)	9.97	35.43	2026(20)	7.9(1)	0.358(6)	2.24(2)	1293(2)	5747(7)	1.006(1)	0.924(0)	0.779(1)	1.035(1)	347.3(5)	359.6(4)
940	4448(2)	9.97	35.88	2030(20)	7.9(1)	0.357(6)	2.23(2)	1293(2)	5752(7)	1.006(1)	0.923(0)	0.776(1)	1.035(1)	349.0(5)	361.2(4)
950	4454(2)	9.97	36.34	2034(20)	7.8(1)	0.355(6)	2.22(2)	1293(2)	5758(7)	1.005(1)	0.922(0)	0.773(1)	1.035(1)	350.6(5)	362.9(4)
960	4460(2)	9.97	36.79	2037(20)	7.8(1)	0.354(6)	2.20(2)	1292(2)	5763(7)	1.005(1)	0.921(0)	0.770(1)	1.035(1)	352.3(5)	364.5(4)
970	4465(2)	9.97	37.24	2041(20)	7.8(1)	0.353(6)	2.19(2)	1292(2)	5768(7)	1.005(1)	0.920(0)	0.767(1)	1.034(1)	354.0(5)	366.1(4)
980	4471(2)	9.97	37.70	2044(20)	7.7(1)	0.351(6)	2.18(2)	1291(2)	5774(7)	1.005(1)	0.919(1)	0.764(1)	1.034(1)	355.6(5)	367.7(4)
990	4476(2)	9.97	38.15	2048(20)	7.7(1)	0.350(6)	2.17(2)	1291(2)	5779(7)	1.005(1)	0.918(1)	0.761(1)	1.034(1)	357.3(5)	369.4(4)
1000	4482(2)	9.97	38.61	2051(21)	7.6(1)	0.349(6)	2.15(2)	1291(2)	5785(8)	1.005(1)	0.916(1)	0.758(1)	1.033(1)	359.0(5)	371.0(4)
1010	4488(2)	9.97	39.07	2055(21)	7.6(1)	0.348(5)	2.14(2)	1290(2)	5790(8)	1.005(1)	0.915(1)	0.755(1)	1.033(1)	360.6(5)	372.6(4)
1020	4493(2)	9.97	39.53	2058(21)	7.6(1)	0.346(5)	2.13(2)	1290(2)	5795(8)	1.005(1)	0.914(1)	0.752(1)	1.033(1)	362.3(5)	374.3(4)
1030	4499(3)	9.96	39.98	2062(21)	7.5(1)	0.345(5)	2.12(2)	1289(2)	5801(8)	1.005(1)	0.913(1)	0.749(1)	1.033(1)	364.0(5)	375.9(4)
1040	4504(3)	9.96	40.44	2065(21)	7.5(1)	0.344(5)	2.11(2)	1289(2)	5806(8)	1.005(1)	0.912(1)	0.746(1)	1.032(1)	365.6(5)	377.5(4)
1050	4510(3)	9.96	40.90	2069(21)	7.5(1)	0.343(6)	2.10(2)	1289(2)	5812(8)	1.005(1)	0.911(1)	0.743(1)	1.032(1)	367.3(5)	379.1(4)
1060	4515(3)	9.96	41.36	2072(21)	7.4(1)	0.341(6)	2.08(2)	1288(2)	5817(8)	1.005(1)	0.910(1)	0.740(1)	1.032(1)	369.0(5)	380.8(4)
1070	4520(3)	9.96	41.81	2075(21)	7.4(1)	0.340(6)	2.07(2)	1288(3)	5822(8)	1.005(1)	0.909(1)	0.738(1)	1.032(1)	370.6(5)	382.4(4)
1080	4526(3)	9.96	42.28	2079(21)	7.4(1)	0.339(6)	2.06(3)	1288(3)	5828(9)	1.005(2)	0.907(1)	0.735(1)	1.031(1)	372.3(5)	384.0(4)
1090	4531(3)	9.96	42.74	2082(21)	7.3(1)	0.338(6)	2.05(3)	1287(3)	5833(9)	1.005(2)	0.906(1)	0.732(1)	1.031(1)	374.0(5)	385.7(4)
1100	4537(3)	9.95	43.20	2086(21)	7.3(1)	0.336(6)	2.04(3)	1287(3)	5839(9)	1.005(2)	0.905(1)	0.729(1)	1.031(1)	375.7(5)	387.3(4)
1110	4542(3)	9.95	43.67	2089(21)	7.3(1)	0.335(6)	2.03(3)	1287(3)	5844(9)	1.005(2)	0.904(1)	0.726(1)	1.031(1)	377.3(5)	389.0(4)
1120	4548(3)	9.95	44.13	2092(21)	7.2(1)	0.334(6)	2.02(3)	1286(3)	5849(9)	1.005(2)	0.903(1)	0.724(1)	1.031(1)	379.0(5)	390.6(4)
1130	4553(3)	9.95	44.59	2096(21)	7.2(1)	0.333(6)	2.01(3)	1286(3)	5855(9)	1.005(2)	0.902(1)	0.721(1)	1.030(1)	380.7(5)	392.2(4)
1140	4559(3)	9.95	45.05	2099(21)	7.2(1)	0.332(6)	2.00(3)	1286(3)	5860(9)	1.005(2)	0.901(1)	0.718(1)	1.030(1)	382.4(5)	393.9(4)
1150	4564(3)	9.94	45.52	2102(21)	7.1(1)	0.330(6)	1.99(3)	1285(3)	5865(10)	1.004(2)	0.900(1)	0.716(1)	1.030(1)	384.0(5)	395.5(4)
1160	4569(3)	9.94	45.98	2106(21)	7.1(1)	0.329(6)	1.98(3)	1285(3)	5871(10)	1.004(2)	0.899(1)	0.713(1)	1.030(1)	385.7(5)	397.1(4)
1170	4575(3)	9.94	46.44	2109(21)	7.1(1)	0.328(6)	1.97(3)	1285(3)	5876(10)	1.004(2)	0.898(1)	0.710(1)	1.029(1)	387.4(5)	398.8(4)
1180	4580(3)	9.94	46.91	2112(21)	7.0(1)	0.327(6)	1.96(3)	1284(3)	5882(10)	1.004(2)	0.897(1)	0.708(1)	1.029(1)	389.0(5)	400.4(4)

1190	4585(3)	9.94	47.38	2115(21)	7.0(1)	0.326(6)	1.95(3)	1284(3)	5887(10)	1.004(2)	0.896(1)	0.705(1)	1.029(1)	390.7(5)	402.1(4)
1200	4591(3)	9.94	47.85	2119(21)	7.0(1)	0.325(6)	1.94(3)	1284(3)	5892(10)	1.004(2)	0.895(1)	0.703(1)	1.029(1)	392.4(5)	403.7(4)
1210	4596(3)	9.94	48.31	2122(21)	6.9(1)	0.324(6)	1.93(3)	1283(3)	5898(10)	1.004(2)	0.894(1)	0.700(1)	1.029(1)	394.1(5)	405.3(4)
1220	4601(3)	9.94	48.78	2125(21)	6.9(1)	0.323(6)	1.92(3)	1283(3)	5903(10)	1.004(2)	0.893(1)	0.697(1)	1.028(1)	395.8(5)	407.0(4)
1230	4607(3)	9.94	49.25	2128(21)	6.9(1)	0.321(6)	1.91(3)	1283(3)	5908(11)	1.004(2)	0.892(1)	0.695(1)	1.028(1)	397.4(5)	408.6(4)
1240	4612(3)	9.94	49.72	2132(22)	6.8(1)	0.320(7)	1.90(3)	1282(3)	5914(11)	1.004(2)	0.891(1)	0.692(1)	1.028(1)	399.1(5)	410.3(4)
1250	4617(3)	9.94	50.18	2135(22)	6.8(1)	0.319(7)	1.89(3)	1282(3)	5919(11)	1.004(2)	0.890(1)	0.690(1)	1.028(1)	400.8(5)	411.9(4)
1260	4623(3)	9.94	50.65	2138(22)	6.8(1)	0.318(7)	1.88(4)	1282(3)	5924(11)	1.004(2)	0.889(1)	0.687(1)	1.028(1)	402.5(5)	413.6(4)
1270	4628(3)	9.94	51.12	2141(22)	6.7(1)	0.317(7)	1.87(4)	1281(3)	5930(11)	1.004(2)	0.888(1)	0.685(1)	1.027(1)	404.1(5)	415.2(4)
1280	4633(3)	9.94	51.59	2144(22)	6.7(1)	0.316(7)	1.86(4)	1281(3)	5935(11)	1.004(2)	0.887(1)	0.682(1)	1.027(1)	405.8(5)	416.8(4)
1290	4638(3)	9.94	52.07	2147(22)	6.7(1)	0.315(7)	1.85(4)	1281(3)	5940(11)	1.004(2)	0.885(1)	0.680(1)	1.027(1)	407.5(5)	418.5(4)
1300	4644(3)	9.94	52.54	2151(22)	6.7(1)	0.314(7)	1.84(4)	1280(3)	5946(11)	1.004(2)	0.884(1)	0.678(1)	1.027(1)	409.2(5)	420.2(4)
1310	4649(3)	9.94	53.01	2154(22)	6.6(2)	0.313(7)	1.83(4)	1280(3)	5951(11)	1.004(2)	0.884(1)	0.675(1)	1.027(1)	410.9(5)	421.8(4)
1320	4654(3)	9.94	53.49	2157(22)	6.6(2)	0.312(7)	1.82(4)	1280(3)	5956(12)	1.004(2)	0.883(1)	0.673(1)	1.026(1)	412.6(5)	423.5(4)
1330	4659(3)	9.93	53.96	2160(22)	6.6(2)	0.311(7)	1.81(4)	1280(3)	5962(12)	1.004(2)	0.882(1)	0.670(1)	1.026(1)	414.2(5)	425.1(4)
1340	4664(3)	9.93	54.43	2163(22)	6.5(2)	0.310(7)	1.80(4)	1279(3)	5967(12)	1.004(2)	0.881(1)	0.668(1)	1.026(1)	415.9(5)	426.8(4)
1350	4670(3)	9.93	54.91	2166(22)	6.5(2)	0.309(7)	1.79(4)	1279(3)	5972(12)	1.003(2)	0.880(1)	0.666(1)	1.026(1)	417.6(5)	428.4(4)
1360	4675(3)	9.93	55.38	2169(22)	6.5(2)	0.308(8)	1.79(4)	1279(3)	5977(12)	1.003(2)	0.879(1)	0.663(1)	1.026(1)	419.3(5)	430.1(4)
1370	4680(3)	9.93	55.85	2172(22)	6.5(2)	0.307(8)	1.78(4)	1278(3)	5983(12)	1.003(2)	0.878(1)	0.661(1)	1.026(1)	420.9(5)	431.7(4)
1380	4685(3)	9.93	56.33	2175(22)	6.4(2)	0.306(8)	1.77(4)	1278(3)	5988(12)	1.003(2)	0.877(1)	0.659(1)	1.025(1)	422.6(5)	433.4(4)
1390	4690(3)	9.93	56.81	2179(22)	6.4(2)	0.305(8)	1.76(4)	1278(3)	5993(12)	1.003(2)	0.876(1)	0.657(2)	1.025(1)	424.3(5)	435.0(4)
1400	4695(3)	9.93	57.29	2182(22)	6.4(2)	0.304(8)	1.75(4)	1278(3)	5999(12)	1.003(2)	0.875(1)	0.654(2)	1.025(1)	426.0(5)	436.7(4)
1410	4701(3)	9.93	57.76	2185(22)	6.3(2)	0.303(8)	1.74(4)	1277(4)	6004(13)	1.003(2)	0.874(1)	0.652(2)	1.025(1)	427.7(5)	438.3(4)
1420	4706(3)	9.93	58.24	2188(22)	6.3(2)	0.302(8)	1.74(4)	1277(4)	6009(13)	1.003(2)	0.873(1)	0.650(2)	1.025(1)	429.4(5)	440.0(4)
1430	4711(4)	9.93	58.72	2191(22)	6.3(2)	0.301(8)	1.73(5)	1277(4)	6014(13)	1.003(2)	0.872(1)	0.647(2)	1.024(1)	431.1(5)	441.7(4)
1440	4716(4)	9.93	59.20	2194(22)	6.3(2)	0.300(8)	1.72(5)	1276(4)	6020(13)	1.003(2)	0.871(1)	0.645(2)	1.024(1)	432.8(5)	443.3(4)
1450	4721(4)	9.93	59.68	2197(22)	6.2(2)	0.299(8)	1.71(5)	1276(4)	6025(13)	1.003(2)	0.870(1)	0.643(2)	1.024(1)	434.5(5)	445.0(4)
1460	4726(4)	9.93	60.16	2200(22)	6.2(2)	0.298(8)	1.70(5)	1276(4)	6030(13)	1.003(2)	0.869(1)	0.641(2)	1.024(1)	436.2(5)	446.6(4)
1470	4731(4)	9.93	60.64	2203(22)	6.2(2)	0.298(9)	1.69(5)	1276(4)	6035(13)	1.003(2)	0.868(1)	0.639(2)	1.024(1)	437.8(5)	448.3(4)
1480	4736(4)	9.93	61.12	2206(22)	6.2(2)	0.297(9)	1.69(5)	1275(4)	6041(13)	1.003(2)	0.867(1)	0.637(2)	1.024(1)	439.5(5)	449.9(4)

1490	4741(4)	9.93	61.60	2209(23)	6.1(2)	0.296(9)	1.68(5)	1275(4)	6046(13)	1.003(2)	0.866(1)	0.634(2)	1.024(1)	441.2(5)	451.6(4)
1500	4747(4)	9.93	62.09	2212(23)	6.1(2)	0.295(9)	1.67(5)	1275(4)	6051(13)	1.003(2)	0.865(1)	0.632(2)	1.023(1)	442.9(5)	453.3(4)
1510	4752(4)	9.93	62.57	2215(23)	6.1(2)	0.294(9)	1.66(5)	1275(4)	6056(14)	1.003(2)	0.864(1)	0.630(2)	1.023(1)	444.6(5)	455.0(4)
1520	4757(4)	9.93	63.05	2217(23)	6.1(2)	0.293(9)	1.66(5)	1274(4)	6062(14)	1.003(2)	0.863(1)	0.628(2)	1.023(1)	446.3(5)	456.6(5)
1530	4762(4)	9.93	63.54	2220(23)	6.0(2)	0.292(9)	1.65(5)	1274(4)	6067(14)	1.003(2)	0.863(1)	0.626(2)	1.023(1)	448.0(5)	458.3(5)
1540	4767(4)	9.93	64.02	2223(23)	6.0(2)	0.291(9)	1.64(5)	1274(4)	6072(14)	1.003(2)	0.862(1)	0.624(2)	1.023(1)	449.7(5)	460.0(5)
1550	4772(4)	9.93	64.50	2226(23)	6.0(2)	0.290(9)	1.63(5)	1274(4)	6077(14)	1.003(2)	0.861(1)	0.622(2)	1.023(1)	451.4(5)	461.6(5)
1560	4777(4)	9.93	64.99	2229(23)	6.0(2)	0.289(9)	1.63(5)	1273(4)	6083(14)	1.002(2)	0.860(1)	0.620(2)	1.022(1)	453.1(5)	463.3(5)
1570	4782(4)	9.93	65.47	2232(23)	5.9(2)	0.289(9)	1.62(5)	1273(4)	6088(14)	1.002(2)	0.859(1)	0.618(2)	1.022(1)	454.8(5)	464.9(5)
1580	4787(4)	9.93	65.96	2235(23)	5.9(2)	0.288(10)	1.61(5)	1273(4)	6093(14)	1.002(2)	0.858(1)	0.616(2)	1.022(1)	456.5(5)	466.6(5)
1590	4792(4)	9.93	66.45	2238(23)	5.9(2)	0.287(10)	1.60(5)	1273(4)	6098(14)	1.002(2)	0.857(1)	0.614(2)	1.022(1)	458.2(5)	468.3(5)
1600	4797(4)	9.93	66.94	2241(23)	5.9(2)	0.286(10)	1.60(5)	1272(4)	6103(14)	1.002(2)	0.856(1)	0.612(2)	1.022(1)	459.9(5)	470.0(5)
1610	4802(4)	9.93	67.43	2243(23)	5.8(2)	0.285(10)	1.59(5)	1272(4)	6109(15)	1.002(2)	0.855(1)	0.610(2)	1.022(1)	461.6(5)	471.7(5)
1620	4807(4)	9.93	67.92	2246(23)	5.8(2)	0.284(10)	1.58(5)	1272(4)	6114(15)	1.002(2)	0.854(1)	0.608(2)	1.022(1)	463.3(5)	473.3(5)
1630	4812(4)	9.93	68.41	2249(23)	5.8(2)	0.283(10)	1.58(5)	1272(4)	6119(15)	1.002(2)	0.854(1)	0.606(2)	1.021(1)	465.0(5)	475.0(5)
1640	4817(4)	9.93	68.90	2252(23)	5.8(2)	0.283(10)	1.57(5)	1271(4)	6124(15)	1.002(2)	0.853(1)	0.604(2)	1.021(1)	466.7(5)	476.7(5)
1650	4822(4)	9.93	69.38	2255(23)	5.7(2)	0.282(10)	1.56(6)	1271(4)	6129(15)	1.002(2)	0.852(1)	0.602(2)	1.021(1)	468.4(5)	478.4(5)
1660	4827(4)	9.93	69.87	2258(23)	5.7(2)	0.281(10)	1.55(6)	1271(4)	6135(15)	1.002(2)	0.851(1)	0.600(2)	1.021(1)	470.1(5)	480.0(5)
1670	4831(4)	9.93	70.36	2260(23)	5.7(2)	0.280(10)	1.55(6)	1271(4)	6140(15)	1.002(2)	0.850(1)	0.598(2)	1.021(1)	471.8(5)	481.7(5)
1680	4836(4)	9.93	70.86	2263(23)	5.7(2)	0.279(10)	1.54(6)	1271(4)	6145(15)	1.002(2)	0.849(1)	0.596(2)	1.021(1)	473.5(5)	483.4(5)
1690	4841(4)	9.93	71.35	2266(23)	5.7(2)	0.279(11)	1.53(6)	1270(4)	6150(15)	1.002(2)	0.848(1)	0.594(2)	1.021(1)	475.3(5)	485.1(5)
1700	4846(4)	9.94	71.85	2269(23)	5.6(2)	0.278(11)	1.53(6)	1270(4)	6155(15)	1.002(2)	0.848(1)	0.592(2)	1.021(1)	477.0(5)	486.8(5)
1710	4851(4)	9.94	72.34	2272(23)	5.6(2)	0.277(11)	1.52(6)	1270(4)	6161(15)	1.002(2)	0.847(1)	0.590(2)	1.020(1)	478.7(5)	488.4(5)
1720	4856(4)	9.94	72.84	2274(24)	5.6(2)	0.276(11)	1.51(6)	1270(4)	6166(15)	1.002(2)	0.846(1)	0.588(2)	1.020(1)	480.4(5)	490.1(5)
1730	4861(4)	9.94	73.33	2277(24)	5.6(2)	0.276(11)	1.51(6)	1269(4)	6171(15)	1.002(2)	0.845(1)	0.586(2)	1.020(1)	482.1(5)	491.8(5)
1740	4866(4)	9.94	73.83	2280(24)	5.5(2)	0.275(11)	1.50(6)	1269(4)	6176(16)	1.002(2)	0.844(1)	0.585(2)	1.020(1)	483.8(5)	493.5(5)
1750	4871(4)	9.95	74.32	2283(24)	5.5(2)	0.274(11)	1.50(6)	1269(4)	6181(16)	1.002(2)	0.843(1)	0.583(2)	1.020(1)	485.5(5)	495.2(5)
1760	4876(4)	9.95	74.82	2285(24)	5.5(2)	0.273(11)	1.49(6)	1269(4)	6186(16)	1.002(2)	0.842(1)	0.581(2)	1.020(1)	487.2(5)	496.9(5)
1770	4880(4)	9.95	75.31	2288(24)	5.5(2)	0.273(11)	1.48(6)	1269(4)	6191(16)	1.001(2)	0.842(1)	0.579(2)	1.020(1)	488.9(5)	498.5(5)
1780	4885(4)	9.95	75.81	2291(24)	5.5(2)	0.272(11)	1.48(6)	1268(4)	6197(16)	1.001(2)	0.841(1)	0.577(2)	1.020(1)	490.7(5)	500.2(5)

1790	4890(4)	9.95	76.31	2294(24)	5.4(2)	0.271(11)	1.47(6)	1268(4)	6202(16)	1.001(2)	0.840(1)	0.575(2)	1.019(1)	492.4(5)	501.9(5)
1800	4895(4)	9.95	76.81	2296(24)	5.4(2)	0.270(11)	1.46(6)	1268(4)	6207(16)	1.001(2)	0.839(1)	0.574(2)	1.019(1)	494.1(5)	503.6(5)
1810	4900(4)	9.95	77.31	2299(24)	5.4(2)	0.270(12)	1.46(6)	1268(4)	6212(16)	1.001(2)	0.838(1)	0.572(2)	1.019(1)	495.8(5)	505.3(5)
1820	4905(4)	9.95	77.81	2302(24)	5.4(2)	0.269(12)	1.45(6)	1268(4)	6217(16)	1.001(2)	0.837(1)	0.570(2)	1.019(1)	497.6(5)	507.0(5)
1830	4910(4)	9.96	78.31	2304(24)	5.4(2)	0.268(12)	1.45(6)	1267(4)	6222(16)	1.001(2)	0.837(1)	0.568(2)	1.019(1)	499.3(5)	508.7(5)
1840	4914(5)	9.96	78.81	2307(24)	5.3(2)	0.267(12)	1.44(6)	1267(4)	6228(16)	1.001(3)	0.836(1)	0.567(2)	1.019(1)	501.0(5)	510.4(5)
1850	4919(5)	9.96	79.31	2310(24)	5.3(2)	0.267(12)	1.43(6)	1267(4)	6233(16)	1.001(3)	0.835(1)	0.565(2)	1.019(1)	502.7(5)	512.1(5)
1860	4924(5)	9.96	79.82	2312(24)	5.3(2)	0.266(12)	1.43(6)	1267(4)	6238(16)	1.001(3)	0.834(1)	0.563(2)	1.019(1)	504.4(5)	513.8(5)
1870	4929(5)	9.96	80.32	2315(24)	5.3(2)	0.265(12)	1.42(6)	1267(4)	6243(16)	1.001(3)	0.833(1)	0.561(2)	1.018(1)	506.1(5)	515.5(5)
1880	4934(5)	9.96	80.82	2318(24)	5.3(2)	0.265(12)	1.42(6)	1266(4)	6248(17)	1.001(3)	0.832(1)	0.560(2)	1.018(1)	507.9(5)	517.2(5)
1890	4939(5)	9.97	81.33	2320(24)	5.2(2)	0.264(12)	1.41(6)	1266(4)	6253(17)	1.001(3)	0.832(1)	0.558(2)	1.018(1)	509.6(5)	518.9(5)
1900	4943(5)	9.97	81.84	2323(24)	5.2(2)	0.263(12)	1.40(6)	1266(4)	6258(17)	1.001(3)	0.831(1)	0.556(2)	1.018(1)	511.4(5)	520.6(5)
1910	4948(5)	9.97	82.34	2326(24)	5.2(2)	0.263(12)	1.40(6)	1266(4)	6263(17)	1.001(3)	0.830(1)	0.554(2)	1.018(1)	513.1(5)	522.3(5)
1920	4953(5)	9.97	82.85	2328(25)	5.2(2)	0.262(12)	1.39(6)	1266(4)	6269(17)	1.001(3)	0.829(1)	0.553(2)	1.018(1)	514.8(5)	524.0(5)
1930	4958(5)	9.98	83.36	2331(25)	5.2(2)	0.261(12)	1.39(6)	1265(4)	6274(17)	1.001(3)	0.828(1)	0.551(2)	1.018(1)	516.6(5)	525.8(5)
1940	4962(5)	9.98	83.86	2334(25)	5.1(2)	0.261(13)	1.38(6)	1265(4)	6279(17)	1.001(3)	0.828(1)	0.549(2)	1.018(1)	518.3(5)	527.5(5)
1950	4967(5)	9.98	84.37	2336(25)	5.1(2)	0.260(13)	1.38(7)	1265(4)	6284(17)	1.001(3)	0.827(1)	0.548(2)	1.018(1)	520.0(5)	529.2(5)
1960	4972(5)	9.99	84.88	2339(25)	5.1(2)	0.260(13)	1.37(7)	1265(4)	6289(17)	1.001(3)	0.826(1)	0.546(2)	1.018(1)	521.7(5)	530.9(5)
1970	4977(5)	9.99	85.38	2341(25)	5.1(3)	0.259(13)	1.36(7)	1265(4)	6294(17)	1.001(3)	0.825(1)	0.544(2)	1.017(1)	523.5(5)	532.6(5)
1980	4981(5)	9.99	85.90	2344(25)	5.1(3)	0.258(13)	1.36(7)	1265(4)	6299(17)	1.001(3)	0.825(1)	0.543(2)	1.017(1)	525.2(5)	534.3(5)
1990	4986(5)	10.00	86.41	2346(25)	5.0(3)	0.258(13)	1.35(7)	1264(4)	6304(17)	1.001(3)	0.824(1)	0.541(2)	1.017(1)	527.0(5)	536.0(5)
2000	4991(5)	10.00	86.92	2349(25)	5.0(3)	0.257(13)	1.35(7)	1264(4)	6309(17)	1.0(3)	0.823(1)	0.540(2)	1.017(1)	528.7(5)	537.7(5)
2010	4996(5)	10.00	87.43	2352(25)	5.0(3)	0.256(13)	1.34(7)	1264(5)	6315(17)	1.0(3)	0.822(1)	0.538(2)	1.017(1)	530.4(5)	539.5(5)
2020	5000(5)	10.00	87.95	2354(25)	5.0(3)	0.256(13)	1.34(7)	1264(5)	6320(17)	1.0(3)	0.821(1)	0.536(2)	1.017(1)	532.2(5)	541.2(5)
2030	5005(5)	10.01	88.46	2357(25)	5.0(3)	0.255(13)	1.33(7)	1264(5)	6325(17)	1.0(3)	0.821(1)	0.535(2)	1.017(1)	533.9(5)	542.9(5)
2040	5010(5)	10.01	88.97	2359(25)	4.9(3)	0.255(13)	1.33(7)	1263(5)	6330(18)	1.0(3)	0.820(1)	0.533(2)	1.017(1)	535.7(5)	544.6(5)
2050	5015(5)	10.01	89.49	2362(25)	4.9(3)	0.254(13)	1.32(7)	1263(5)	6335(18)	1.0(3)	0.819(1)	0.532(2)	1.017(1)	537.4(5)	546.3(5)
2060	5019(5)	10.02	90.00	2364(25)	4.9(3)	0.253(13)	1.32(7)	1263(5)	6340(18)	1.0(3)	0.818(1)	0.530(2)	1.017(1)	539.2(5)	548.1(5)
2070	5024(5)	10.02	90.51	2367(25)	4.9(3)	0.253(13)	1.31(7)	1263(5)	6346(18)	1.0(3)	0.818(1)	0.528(2)	1.016(1)	540.9(5)	549.8(5)
2080	5029(5)	10.02	91.03	2369(25)	4.9(3)	0.252(14)	1.31(7)	1263(5)	6352(18)	1.0(3)	0.817(1)	0.527(2)	1.016(1)	542.7(5)	551.5(5)

2090	5033(5)	10.03	91.55	2372(26)	4.9(3)	0.251(14)	1.30(7)	1263(5)	6357(18)	1.0(3)	0.816(1)	0.525(2)	1.016(1)	544.4(5)	553.2(5)
2100	5038(5)	10.03	92.07	2374(26)	4.8(3)	0.251(14)	1.30(7)	1263(5)	6363(18)	1.0(3)	0.815(1)	0.524(2)	1.016(1)	546.2(5)	555.0(5)
2110	5043(5)	10.03	92.59	2377(26)	4.8(3)	0.250(14)	1.29(7)	1263(5)	6368(18)	1.0(3)	0.814(1)	0.522(2)	1.016(1)	547.9(5)	556.7(5)
2120	5048(5)	10.03	93.11	2379(26)	4.8(3)	0.250(14)	1.29(7)	1263(5)	6374(18)	1.001(3)	0.814(1)	0.521(2)	1.016(1)	549.7(5)	558.4(5)
2130	5052(5)	10.04	93.63	2382(26)	4.8(3)	0.249(14)	1.28(7)	1263(5)	6379(18)	1.001(3)	0.813(1)	0.519(2)	1.016(1)	551.4(5)	560.2(5)
2140	5057(5)	10.04	94.15	2384(26)	4.8(3)	0.248(14)	1.28(7)	1263(5)	6385(18)	1.001(3)	0.812(1)	0.518(2)	1.016(1)	553.2(5)	561.9(5)
2150	5062(5)	10.04	94.67	2387(26)	4.7(3)	0.248(14)	1.27(7)	1263(5)	6390(18)	1.001(3)	0.811(1)	0.516(2)	1.016(1)	555.0(5)	563.7(5)
2160	5066(5)	10.05	95.19	2389(26)	4.7(3)	0.247(14)	1.27(7)	1262(5)	6396(18)	1.001(3)	0.811(1)	0.515(2)	1.016(1)	556.7(5)	565.4(5)
2170	5071(5)	10.05	95.71	2392(26)	4.7(3)	0.247(14)	1.26(7)	1262(5)	6401(19)	1.001(3)	0.810(1)	0.513(2)	1.015(1)	558.5(5)	567.1(5)
2180	5076(5)	10.05	96.24	2394(26)	4.7(3)	0.246(14)	1.26(7)	1262(5)	6407(19)	1.001(3)	0.809(1)	0.512(2)	1.015(1)	560.2(5)	568.9(5)
2190	5080(5)	10.06	96.77	2397(26)	4.7(3)	0.246(14)	1.25(7)	1262(5)	6413(19)	1.001(3)	0.808(1)	0.510(2)	1.015(1)	562.0(5)	570.6(5)
2200	5085(5)	10.06	97.29	2399(26)	4.7(3)	0.245(14)	1.25(7)	1262(5)	6418(19)	1.001(3)	0.808(1)	0.509(2)	1.015(1)	563.8(5)	572.4(5)
2210	5090(5)	10.07	97.82	2402(26)	4.6(3)	0.244(14)	1.24(7)	1262(5)	6424(19)	1.001(3)	0.807(1)	0.507(2)	1.015(1)	565.6(5)	574.1(5)
2220	5094(5)	10.07	98.35	2404(26)	4.6(3)	0.244(14)	1.24(7)	1262(5)	6429(19)	1.001(3)	0.806(1)	0.506(2)	1.015(1)	567.3(5)	575.9(5)
2230	5099(5)	10.08	98.87	2407(27)	4.6(3)	0.243(15)	1.23(7)	1262(5)	6435(19)	1.001(3)	0.806(1)	0.504(2)	1.015(1)	569.1(5)	577.6(5)
2240	5103(5)	10.08	99.40	2409(27)	4.6(3)	0.243(15)	1.23(7)	1262(5)	6440(19)	1.001(3)	0.805(1)	0.503(2)	1.015(1)	570.9(5)	579.4(5)
2250	5108(5)	10.09	99.93	2411(27)	4.6(3)	0.242(15)	1.22(7)	1262(5)	6446(19)	1.001(3)	0.804(1)	0.501(2)	1.015(1)	572.6(5)	581.1(5)
2260	5113(5)	10.09	100.46	2414(27)	4.6(3)	0.242(15)	1.22(7)	1262(5)	6451(19)	1.001(3)	0.803(1)	0.500(2)	1.015(1)	574.4(5)	582.9(5)
2270	5117(5)	10.10	100.98	2416(27)	4.5(3)	0.241(15)	1.21(7)	1262(5)	6457(19)	1.001(3)	0.803(1)	0.499(2)	1.015(1)	576.2(5)	584.6(5)
2280	5122(5)	10.11	101.52	2419(27)	4.5(3)	0.241(15)	1.21(7)	1262(5)	6462(19)	1.001(3)	0.802(1)	0.497(2)	1.015(1)	578.0(5)	586.4(5)
2290	5127(5)	10.11	102.05	2421(27)	4.5(3)	0.240(15)	1.21(7)	1262(5)	6468(19)	1.001(3)	0.801(1)	0.496(2)	1.014(1)	579.8(5)	588.2(5)
2300	5131(5)	10.12	102.59	2424(27)	4.5(3)	0.240(15)	1.20(7)	1262(5)	6473(19)	1.001(3)	0.800(1)	0.494(2)	1.014(1)	581.6(5)	589.9(5)
2310	5136(5)	10.12	103.12	2426(27)	4.5(3)	0.239(15)	1.20(7)	1261(5)	6479(19)	1.001(3)	0.800(1)	0.493(2)	1.014(1)	583.3(5)	591.7(5)
2320	5141(5)	10.13	103.66	2428(27)	4.5(3)	0.239(15)	1.19(7)	1261(5)	6484(19)	1.001(3)	0.799(1)	0.492(2)	1.014(1)	585.1(5)	593.5(5)
2330	5145(5)	10.14	104.19	2431(27)	4.4(3)	0.238(15)	1.19(7)	1261(5)	6490(19)	1.001(3)	0.798(1)	0.490(2)	1.014(1)	586.9(5)	595.2(5)
2340	5150(6)	10.14	104.73	2433(27)	4.4(3)	0.238(15)	1.18(7)	1261(5)	6495(19)	1.001(3)	0.798(1)	0.489(2)	1.014(1)	588.7(5)	597.0(5)
2350	5154(6)	10.15	105.26	2435(28)	4.4(3)	0.237(15)	1.18(7)	1261(5)	6501(19)	1.001(3)	0.797(1)	0.487(2)	1.014(1)	590.5(5)	598.8(5)
2360	5159(6)	10.15	105.80	2438(28)	4.4(3)	0.237(15)	1.17(7)	1261(5)	6506(19)	1.001(3)	0.796(1)	0.486(2)	1.014(1)	592.3(5)	600.5(5)
2370	5163(6)	10.16	106.33	2440(28)	4.4(3)	0.236(15)	1.17(7)	1261(5)	6511(19)	1.001(3)	0.795(1)	0.485(2)	1.014(1)	594.1(5)	602.3(5)
2380	5168(6)	10.17	106.88	2443(28)	4.4(3)	0.236(15)	1.17(7)	1261(5)	6517(19)	1.001(3)	0.795(1)	0.483(2)	1.014(1)	595.9(5)	604.1(5)

2390	5173(6)	10.17	107.42	2445(28)	4.4(3)	0.235(16)	1.16(7)	1261(5)	6522(19)	1.001(3)	0.794(1)	0.482(2)	1.014(1)	597.7(5)	605.9(5)
2400	5177(6)	10.18	107.96	2447(28)	4.3(3)	0.235(16)	1.16(7)	1261(5)	6528(20)	1.001(3)	0.793(1)	0.481(2)	1.014(1)	599.5(5)	607.7(5)
2410	5182(6)	10.19	108.51	2450(28)	4.3(3)	0.235(16)	1.15(7)	1261(5)	6533(20)	1.001(3)	0.793(1)	0.479(2)	1.014(1)	601.3(5)	609.5(5)
2420	5187(6)	10.19	109.05	2452(28)	4.3(3)	0.234(16)	1.15(7)	1261(5)	6539(20)	1.001(3)	0.792(1)	0.478(2)	1.013(1)	603.1(5)	611.2(5)
2430	5191(6)	10.20	109.59	2454(28)	4.3(3)	0.234(16)	1.14(7)	1261(5)	6544(20)	1.001(3)	0.791(1)	0.477(2)	1.013(1)	604.9(5)	613.0(5)
2440	5196(6)	10.21	110.14	2457(28)	4.3(3)	0.233(16)	1.14(7)	1261(5)	6550(20)	1.001(3)	0.791(1)	0.475(2)	1.013(1)	606.7(5)	614.8(5)
2450	5200(6)	10.22	110.68	2459(28)	4.3(3)	0.233(16)	1.14(7)	1261(5)	6555(20)	1.001(3)	0.790(1)	0.474(2)	1.013(1)	608.5(5)	616.6(5)
2460	5205(6)	10.22	111.22	2461(29)	4.2(3)	0.232(16)	1.13(7)	1261(5)	6561(20)	1.001(3)	0.789(1)	0.473(2)	1.013(1)	610.3(5)	618.4(5)
2470	5209(6)	10.23	111.77	2464(29)	4.2(3)	0.232(16)	1.13(7)	1260(5)	6566(20)	1.001(3)	0.788(1)	0.471(2)	1.013(1)	612.1(5)	620.2(5)
2480	5214(6)	10.24	112.32	2466(29)	4.2(3)	0.232(16)	1.12(7)	1260(5)	6572(20)	1.001(3)	0.788(1)	0.470(2)	1.013(1)	614.0(5)	622.0(5)
2490	5219(6)	10.25	112.87	2468(29)	4.2(3)	0.231(16)	1.12(7)	1260(5)	6577(20)	1.001(3)	0.787(1)	0.469(2)	1.013(1)	615.8(5)	623.8(5)
2500	5223(6)	10.25	113.42	2471(29)	4.2(3)	0.231(16)	1.12(7)	1260(5)	6582(20)	1.002(3)	0.786(1)	0.467(2)	1.013(1)	617.6(5)	625.6(5)
2510	5228(6)	10.26	113.98	2473(29)	4.2(3)	0.230(16)	1.11(7)	1260(5)	6588(20)	1.002(3)	0.786(1)	0.466(2)	1.013(1)	619.5(5)	627.4(5)
2520	5232(6)	10.27	114.53	2475(29)	4.2(3)	0.230(16)	1.11(7)	1260(5)	6593(20)	1.002(3)	0.785(1)	0.465(2)	1.013(1)	621.3(5)	629.2(5)
2530	5237(6)	10.28	115.08	2478(29)	4.1(3)	0.229(16)	1.10(8)	1260(5)	6599(20)	1.002(3)	0.784(1)	0.464(2)	1.013(1)	623.1(5)	631.0(5)
2540	5241(6)	10.29	115.63	2480(29)	4.1(3)	0.229(16)	1.10(8)	1260(5)	6604(20)	1.002(3)	0.784(1)	0.462(2)	1.013(1)	625.0(5)	632.9(5)
2550	5246(6)	10.29	116.19	2482(29)	4.1(3)	0.229(16)	1.10(8)	1260(5)	6610(20)	1.002(3)	0.783(1)	0.461(2)	1.013(1)	626.8(5)	634.7(5)
2560	5251(6)	10.30	116.74	2484(29)	4.1(3)	0.228(17)	1.09(8)	1260(5)	6615(20)	1.002(3)	0.782(1)	0.460(2)	1.012(1)	628.6(5)	636.5(5)
2570	5255(6)	10.31	117.29	2487(30)	4.1(3)	0.228(17)	1.09(8)	1260(5)	6620(20)	1.002(3)	0.782(1)	0.459(2)	1.012(1)	630.4(5)	638.3(5)
2580	5260(6)	10.32	117.85	2489(30)	4.1(3)	0.227(17)	1.08(8)	1260(5)	6626(20)	1.002(3)	0.781(1)	0.457(2)	1.012(1)	632.3(5)	640.1(5)
2590	5264(6)	10.33	118.42	2491(30)	4.1(3)	0.227(17)	1.08(8)	1260(5)	6631(20)	1.002(3)	0.780(1)	0.456(2)	1.012(1)	634.2(5)	641.9(5)
2600	5269(6)	10.34	118.98	2494(30)	4.0(3)	0.227(17)	1.08(8)	1260(5)	6637(20)	1.002(3)	0.780(1)	0.455(2)	1.012(1)	636.0(5)	643.8(5)
2610	5273(6)	10.35	119.54	2496(30)	4.0(3)	0.226(17)	1.07(8)	1260(5)	6642(20)	1.002(3)	0.779(1)	0.454(2)	1.012(1)	637.9(5)	645.6(5)
2620	5278(6)	10.36	120.10	2498(30)	4.0(3)	0.226(17)	1.07(8)	1260(5)	6648(21)	1.002(3)	0.778(1)	0.452(2)	1.012(1)	639.7(5)	647.4(5)
2630	5283(6)	10.37	120.67	2500(30)	4.0(3)	0.226(17)	1.07(8)	1259(5)	6653(21)	1.002(3)	0.778(1)	0.451(2)	1.012(1)	641.6(5)	649.3(5)
2640	5287(6)	10.38	121.23	2503(30)	4.0(3)	0.225(17)	1.06(8)	1259(5)	6659(21)	1.002(3)	0.777(1)	0.450(2)	1.012(1)	643.4(5)	651.1(5)
2650	5292(6)	10.39	121.79	2505(30)	4.0(3)	0.225(17)	1.06(8)	1259(5)	6664(21)	1.002(3)	0.776(1)	0.449(2)	1.012(1)	645.3(5)	652.9(5)
2660	5296(6)	10.40	122.35	2507(31)	4.0(3)	0.225(17)	1.05(8)	1259(5)	6669(21)	1.002(3)	0.776(1)	0.447(2)	1.012(1)	647.1(5)	654.8(5)
2670	5301(6)	10.41	122.92	2509(31)	3.9(3)	0.224(17)	1.05(8)	1259(5)	6675(21)	1.002(3)	0.775(1)	0.446(2)	1.012(1)	649.0(5)	656.6(5)
2680	5305(6)	10.42	123.49	2512(31)	3.9(3)	0.224(17)	1.05(8)	1259(5)	6680(21)	1.002(3)	0.774(1)	0.445(2)	1.012(1)	650.8(5)	658.5(5)

2690	5310(6)	10.43	124.06	2514(31)	3.9(3)	0.224(17)	1.04(8)	1259(5)	6686(21)	1.002(3)	0.774(1)	0.444(2)	1.012(1)	652.7(5)	660.3(5)
2700	5314(6)	10.44	124.63	2516(31)	3.9(3)	0.223(17)	1.04(8)	1259(5)	6691(21)	1.002(3)	0.773(1)	0.443(2)	1.012(1)	654.6(5)	662.2(5)
2710	5319(6)	10.45	125.20	2518(31)	3.9(3)	0.223(17)	1.04(8)	1259(5)	6697(21)	1.002(3)	0.772(1)	0.441(2)	1.012(1)	656.5(5)	664.0(5)
2720	5323(6)	10.46	125.77	2520(31)	3.9(3)	0.223(17)	1.03(8)	1259(5)	6702(21)	1.002(3)	0.772(1)	0.440(2)	1.011(1)	658.4(5)	665.9(5)
2730	5328(6)	10.47	126.35	2523(31)	3.9(3)	0.222(18)	1.03(8)	1259(5)	6707(21)	1.002(3)	0.771(1)	0.439(2)	1.011(1)	660.2(5)	667.8(5)
2740	5332(6)	10.48	126.92	2525(31)	3.9(3)	0.222(18)	1.03(8)	1259(5)	6713(21)	1.002(3)	0.770(1)	0.438(2)	1.011(1)	662.1(5)	669.6(5)
2750	5337(6)	10.49	127.49	2527(32)	3.8(3)	0.222(18)	1.02(8)	1259(5)	6718(21)	1.002(3)	0.770(1)	0.437(2)	1.011(1)	664.0(5)	671.5(5)
2760	5342(6)	10.51	128.07	2529(32)	3.8(3)	0.221(18)	1.02(8)	1259(5)	6724(21)	1.002(3)	0.769(1)	0.436(2)	1.011(1)	665.9(5)	673.4(5)
2770	5346(6)	10.52	128.65	2532(32)	3.8(3)	0.221(18)	1.01(8)	1259(5)	6729(21)	1.002(3)	0.768(1)	0.434(2)	1.011(1)	667.8(5)	675.2(5)
2780	5351(6)	10.53	129.23	2534(32)	3.8(3)	0.221(18)	1.01(8)	1259(5)	6735(21)	1.002(3)	0.768(1)	0.433(2)	1.011(1)	669.7(5)	677.1(5)
2790	5355(6)	10.54	129.82	2536(32)	3.8(3)	0.221(18)	1.01(8)	1259(5)	6740(21)	1.002(3)	0.767(1)	0.432(2)	1.011(1)	671.6(5)	679.0(5)
2800	5360(6)	10.56	130.40	2538(32)	3.8(3)	0.220(18)	1.00(8)	1259(5)	6745(21)	1.002(3)	0.766(1)	0.431(2)	1.011(1)	673.5(5)	680.9(5)

#: taken from PREM [Dziewonski and Anderson, 1981].

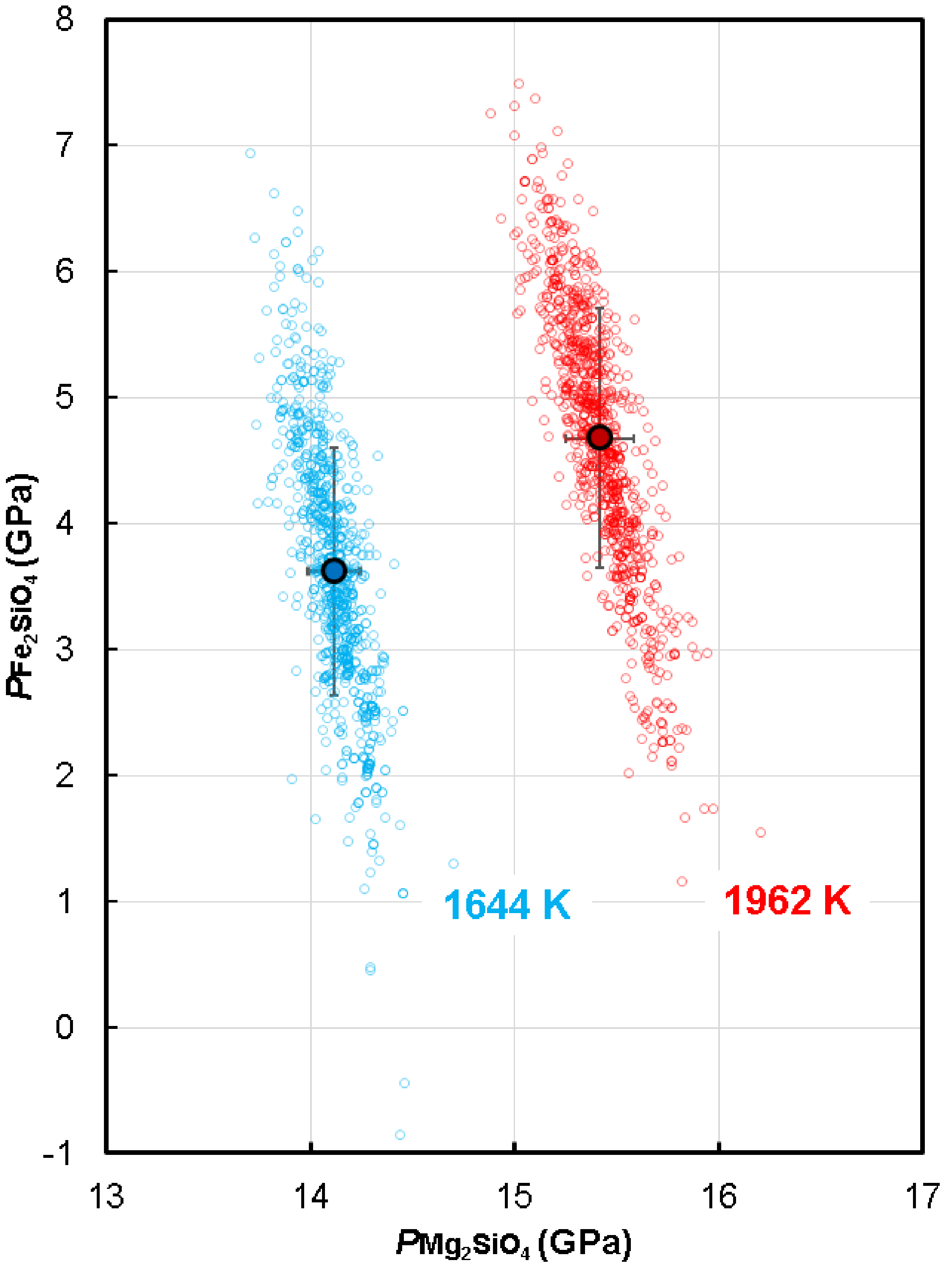

Figure S1. Correlation of the endmember transition pressures of the olivine wadsleyite transition. Determined by the data from Katsura *et al.* [2004a], corrected using Nishihara *et al.*'s [2020] thermocouple correction. Each point show the transition pressure obtained in each replica data set of the Monte Carlo simulation.

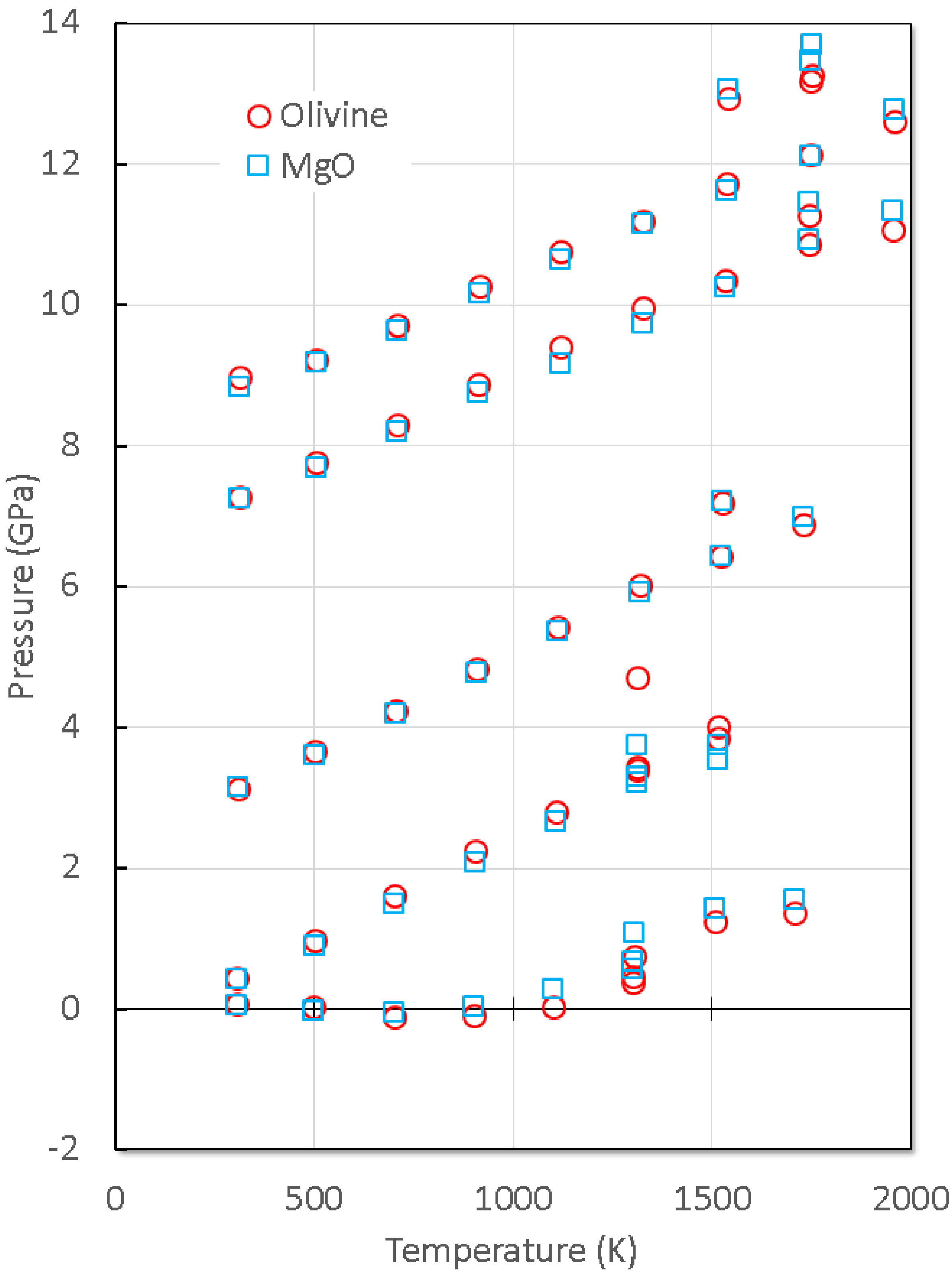

Figure S2. Comparison of the pressures using Tange *et al.*'s [2009] MgO and the current study's olivine EOS's.

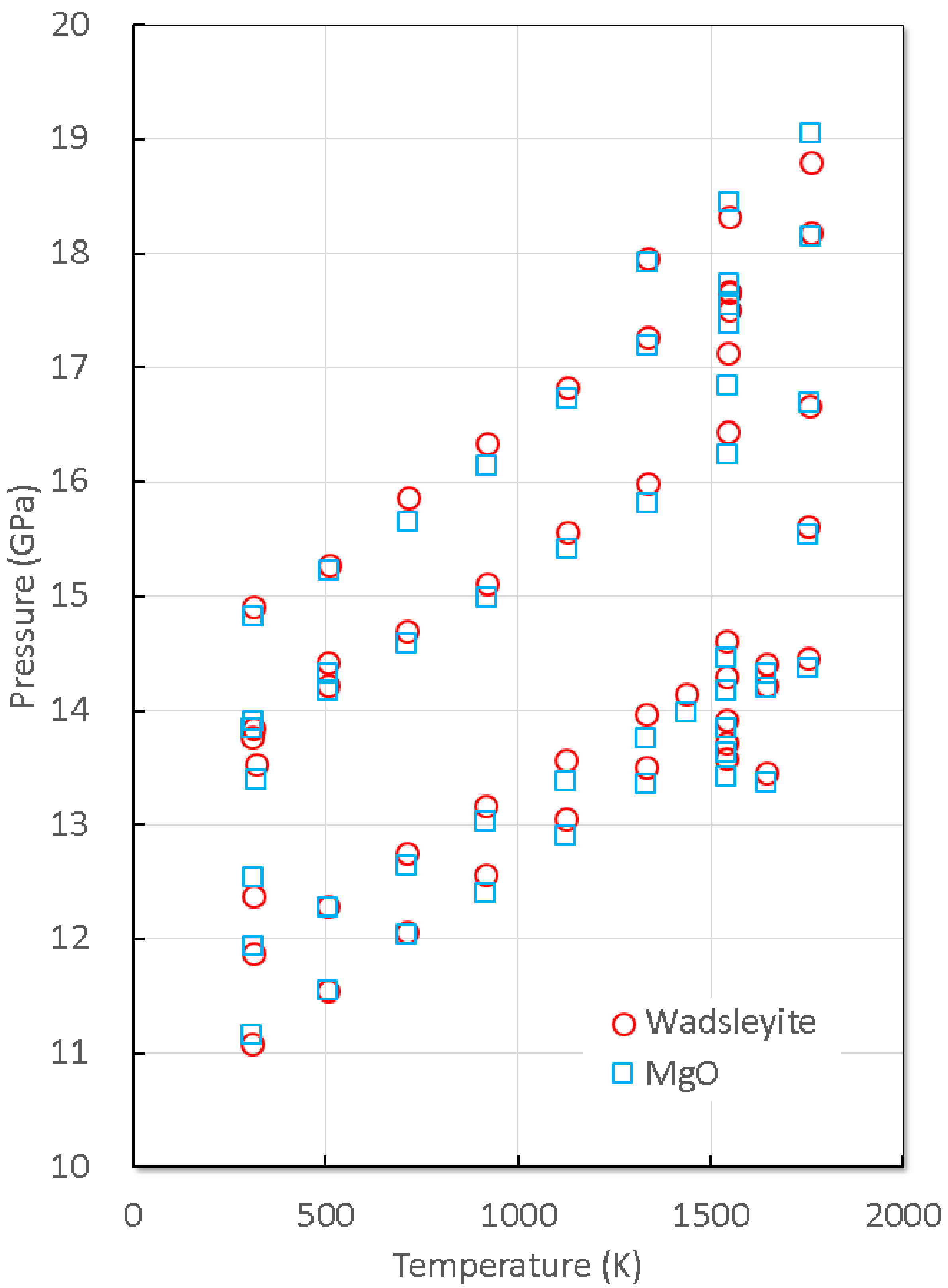

Figure S3. Comparison of the pressures using Tange *et al.*'s [2009] MgO and the current study's wadsleyite EOS's.

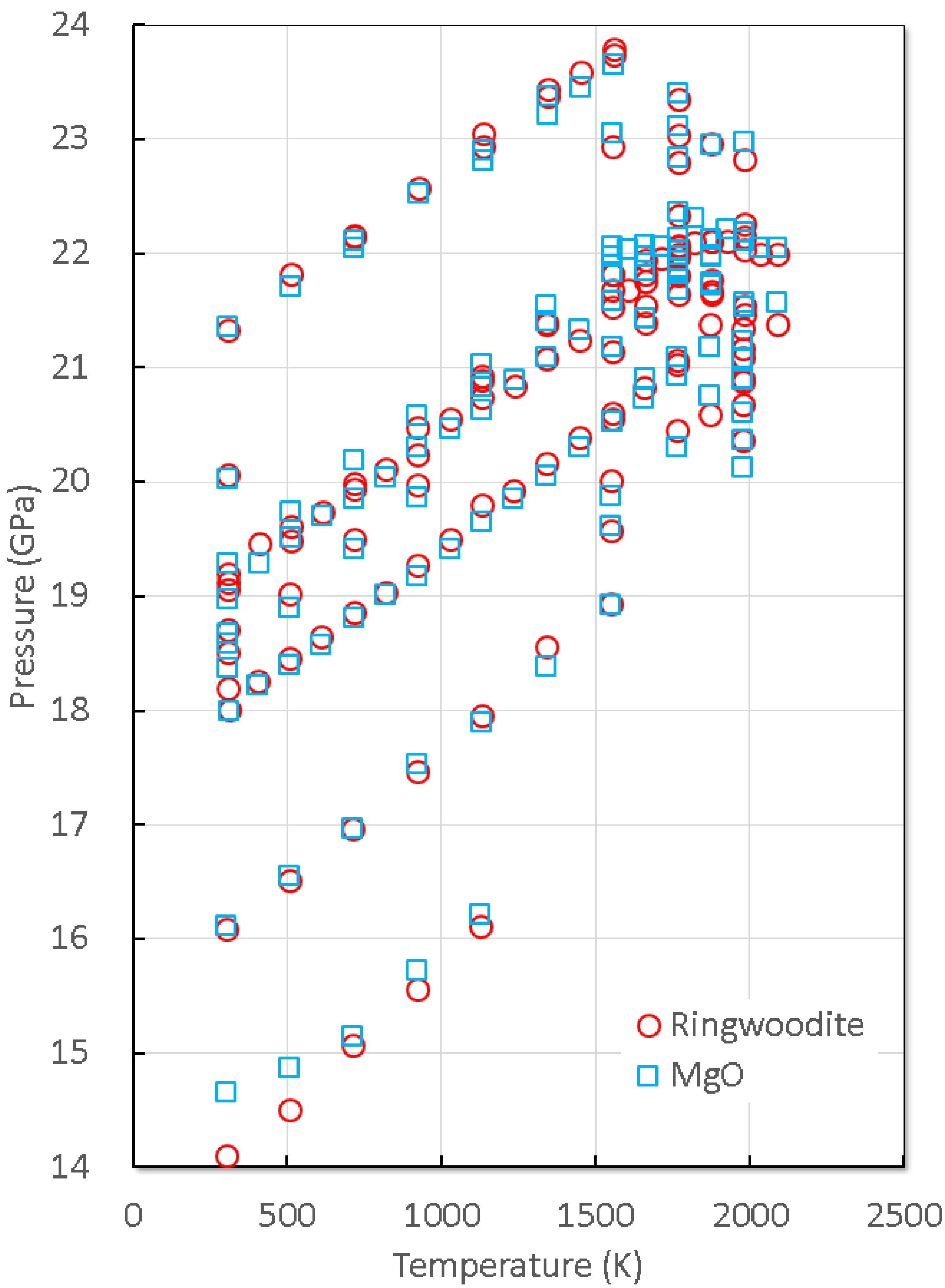

585

586 **Figure S4.** Comparison of the pressures using Tange *et al.*'s [2009] MgO and the current

587 study's ringwoodite EOS's.

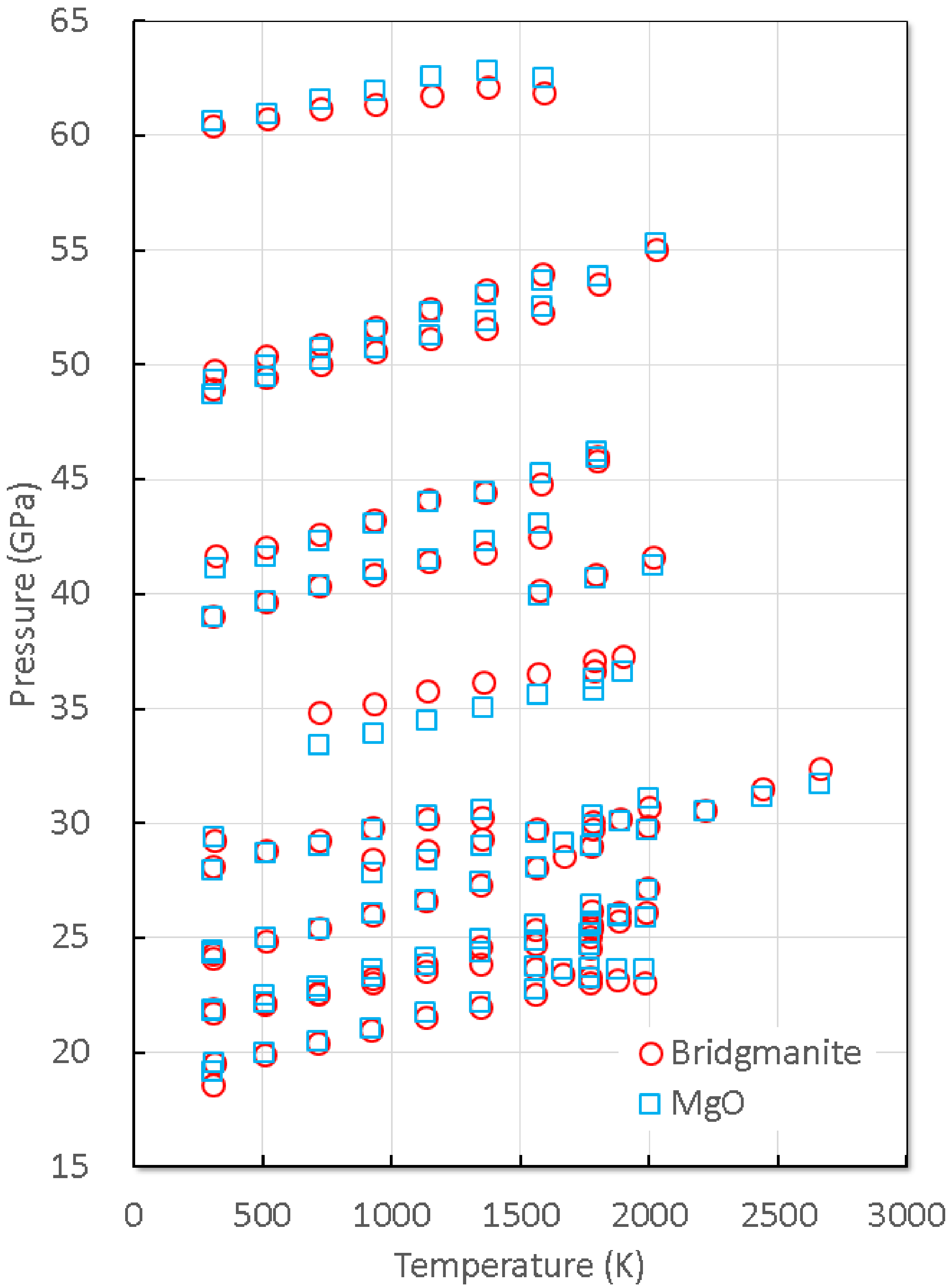

Figure S5. Comparison of the pressures using Tange *et al.*'s [2009] MgO and the current study's bridgmanite EOS's.

.

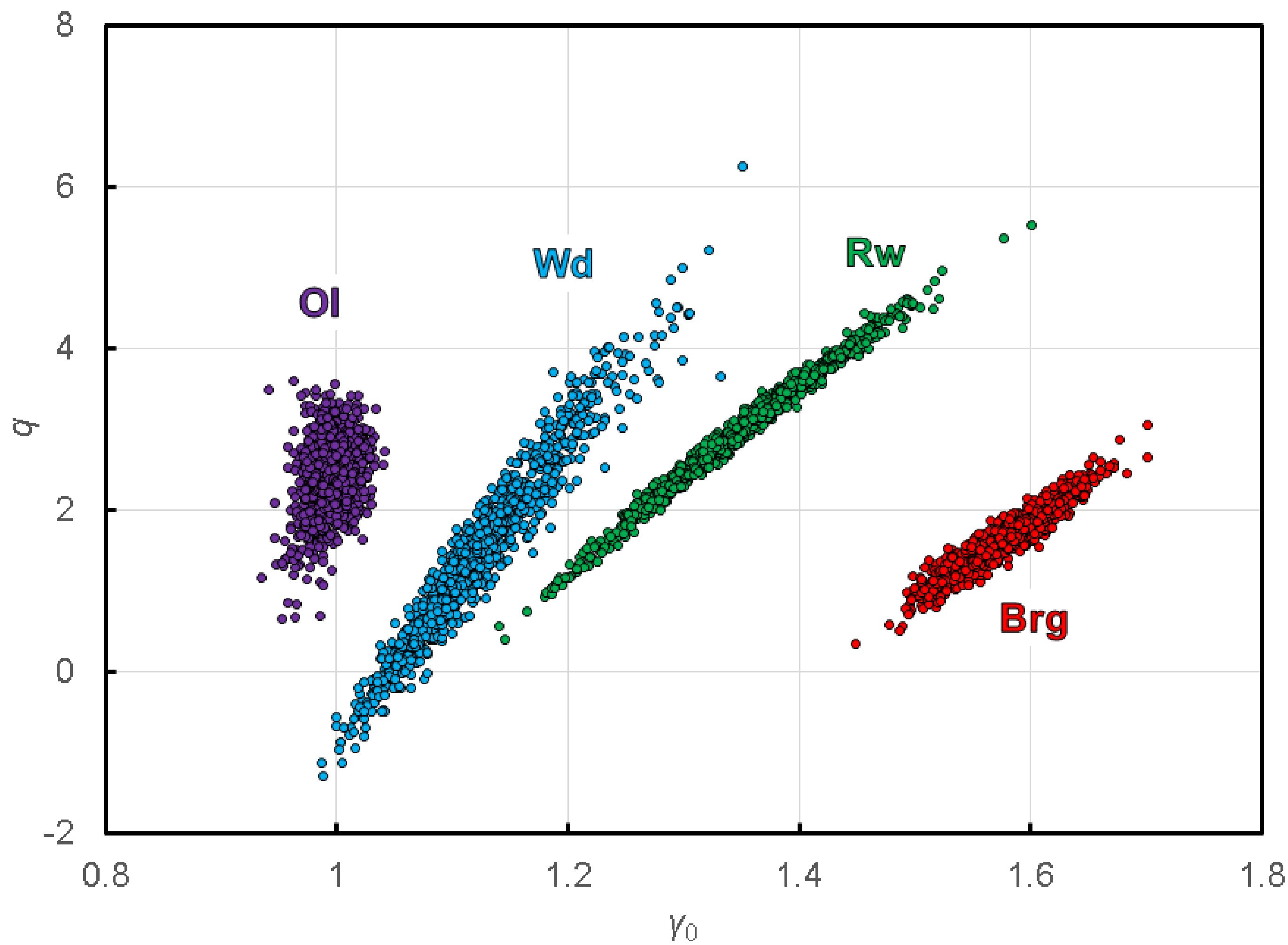

Figure S6. The correlations of γ_0 and q. Violet: olivine, blue: wadsleyite, green: ringwoodite, red: bridgmanite. Original data from Katsura *et al.* [2004a; 2009a; 2009b; 2009c] are corrected using Nishihara *et al.*'s [2020] thermocouple correction.